ornl

ORNL/TM-13757

OAK RIDGE
NATIONAL
LABORATORY

LOCKHEED MARTIN

Compressive Creep Performance and High Temperature Dimensional Stability of Conventional Silica Refractories

A. A. Wereszczak
M. Karakus
K. C. Liu
B. A. Pint
R. E. Moore
T. P. Kirkland

March 1999

MANAGED AND OPERATED BY
LOCKHEED MARTIN ENERGY RESEARCH CORPORATION
FOR THE UNITED STATES
DEPARTMENT OF ENERGY

ORNL-27 (3-96)

DISCLAIMER

ORNL/TM-13757

COMPRESSIVE CREEP PERFORMANCE AND HIGH TEMPERATURE DIMENSIONAL STABILITY OF CONVENTIONAL SILICA REFRACTORIES

A. A. Wereszczak[1,2] and M. Karakus[2,3]

with K. C. Liu,[1,4] B. A. Pint,[1,4] R. E. Moore,[3,4] and T. P. Kirkland [1,4]

Prepared for the
Advanced Industrial Materials Program and the Glass Vision Team
Office of Industrial Technologies
Assistant Secretary for Energy Efficiency and Renewable Energy
U.S. Department of Energy
ED 18 05 00 0

Prepared by the
OAK RIDGE NATIONAL LABORATORY
Oak Ridge, Tennessee 37831-6285
managed by
LOCKHEED MARTIN ENERGY RESEARCH CORP.
for the
U.S. DEPARTMENT OF ENERGY
under contract DE-AC05-96OR22464

---

1 Oak Ridge National Laboratory, Metals and Ceramics Division, Oak Ridge, TN.
2 Principal Investigator.
3 University of Missouri, Ceramic Engineering Department, Rolla, MO.
4 Contributing Investigator.

EXECUTIVE SUMMARY

Compressive creep testing of six commercially available conventional silica refractories was performed at 1550-1650°C and at static stresses between 0.2-0.6 MPa. These refractories were examined because they are used in glass production furnace superstructures. Corrosion resistance analyses were also performed on these six materials. Measurements were also made that tracked their dimensional stability, phase content, microstructure, and composition as a function of temperature. The techniques used for these characterizations and their respective analyses are described.

An intent of this study was to provide objective and factual results whose interpretations were meant to be left up to the report's reader. The salient observations and conclusions were:

- The amount of compressive creep of Gen-Sil, Stella GGS, Vega, Vega H, and Harbison-Walker's new developmental brand (flux factors less than 0.5% or "Type A" silica for all five of these brands) conventional silica was negligible at temperatures 1550-1650°C (2820-3000°F) and at compressive stresses 0.2-0.6 MPa (29-57 psi).
- The compressive creep of SI96AU (flux factor greater than 0.5% or "Type B" silica) conventional silica was negligible at 1550°C. However, SI96AU deformed (contracted) by more than 20% at 1600°C and stresses between 0.2-0.6 MPa. This behavior was inferior to that of the other five tested brands.
- The compressive creep rates of all six brands were not able to be represented as a function of temperature and compressive stress using the conventionally used Arrhenius Norton-Bailey creep equation (*i.e.*, the Arrhenius power-law creep model). Concurrently active mechanism(s), other than creep, resulted in larger or oppositely anticipated dimensional changes than those produced by creep; this effect limited the ability to identify or interpret the lesser-active creep mechanism in these silica refractories. A new alternative empirical model likely needs to be developed to represent these dimensional changes as a function of time and temperature.
- The change in dimensions of the compressively crept specimens indicated that their size (both diameter and length) had actually increased as a consequence of the employed creep test conditions. The increases in diameter and length of the creep specimens were between 0.35-1.0%. All six brands showed this expansion effect.
- The secondary phase constituents remained in all brands when they were tested at 1550°C (cumulative time at temperature approximately 250 hours). A fraction of these phases vaporized out of the specimens at 1600°C (slight glass bubbling on the specimen and fixturing). This phenomenon was quite severe at 1650°C. The density changes in the crept

specimens (a net effect of the volume expansion and loss in secondary phase mass) ranged from a decrease of 1.6 to 3.9% with a subtle trend of greater density decreases at higher test temperatures. The density decreases among the six brands were statistically equivalent within the data scatter.

- The cause of the volume expansion was not conclusively identified. We speculate that the volume expansion is due to the high temperature process involving the conversion of tridymite to cristobalite, and the consequential growth of the residual pores and the original cristobalite aggregates in the silicas between 1550-1650°C.
- Unstressed or "aged" silica refractory specimens from all six materials also exhibited loss of mass, dimensional increases, and density decreases between 1550-1650°C.
  - The mass losses of the six brands at 1550 and 1600°C were equivalent; however, some silica brands lost more mass than others at 1650°C: Harbison-Walker's developmental brand lost approximately 0.1% of its mass; SI96AU lost ≈ 0.2%; Vega H lost ≈ 0.3%; Gen-Sil lost ≈ 0.5%; Vega lost ≈ 1.0%; and Stella GGS lost ≈ 1.5%. The majority of the mass loss for all brands occurred in less than 25 hours.
  - The dimensional increases of the silica specimens were a function of temperature. Additionally, some brands expanded more than others. The ranges of expansion were ≈ 1-2.5% at 1550°C, ≈ 2.25-3.75% at 1600°C, and ≈ 3.5-6% at 1650°C. Harbison-Walker's developmental brand expanded the least amount at all three temperatures followed by Gen-Sil. The ascending order of expansion for the other four brands varied with temperature. Stella GGS expanded the most at 1550°C (≈ 2.5%), SI96AU expanded the most at 1600°C (≈ 3.75%), and Vega expanded the most at 1650°C (≈ 6%).
  - The density decreases of the silica specimens were a function of temperature. Additionally, some brands became less dense than others. The changes in density are a consequence of the above described changes in mass and volume. The ranges of density decreases were ≈ 1-2.75% at 1550°C, ≈ 2.25-4.0% at 1600°C, and ≈ 3.5-7.0% at 1650°C. The density of Harbison-Walker's developmental brand changed the least of the six brands at all three temperatures. The ascending order of density for the other five brands varied with temperature. The density of Stella GGS decreased the most at 1550°C (≈ 2.75%); that for SI96AU decreased the most at 1600°C (≈ 4%); and that for Vega decreased the most at 1650°C (≈ 7%).
- The corrosion resistances of the six silicas were statistically equivalent when they were exposed to sodium carbonate at 1400°C (2550°F) for 24 hours. The amount of recession increased linearly with temperature between 1250-1450°C for the Gen-Sil silica.

TABLE OF CONTENTS

LIST OF FIGURES

LIST OF TABLES

1. INTRODUCTION

Furnace designers and refractory engineers recognize that optimized furnace superstructure design and refractory selection are needed as glass production furnaces are continually striving toward greater output and efficiencies. Harsher operating conditions test refractories to the limit, while changing production technology (such as the conversion to oxy-fuel from traditional air-fuel firing) can alter the way the materials perform [1-3]. Refractories for both oxy- and air-fuel fired furnace superstructures (see Fig. 1) are subjected to high temperatures during service that may cause them to excessively creep or subside if the refractory material is not creep resistant, or if it is subjected to high stress, or both. Furnace designers can ensure that superstructure structural integrity is maintained if the creep behavior of the refractory material is well understood and well represented by appropriate engineering creep models.

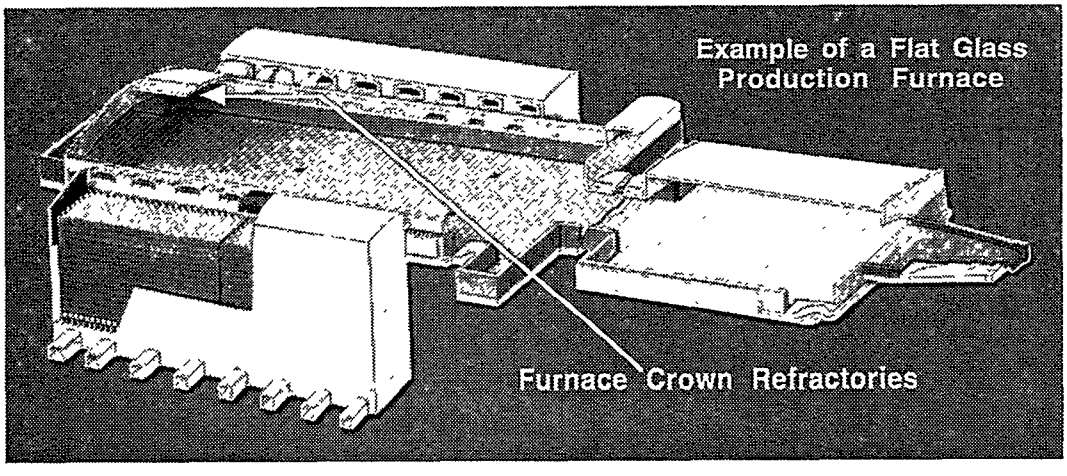

Fig. 1. Superstructure refractories in glass production furnaces.

Several issues limit the abilities of furnace designers to (1) choose the optimum refractory for their applications, (2) optimize the engineering design, or (3) predict the service mechanical integrity of their furnace superstructures. Published engineering creep data are essentially non-existent for almost all commercially available refractories used for glass furnace superstructures. The limited data that do exist are supplied by the various refractory suppliers. Unfortunately, these suppliers generally have different ways of conducting their mechanical testing and they also interpret and report their data differently; this makes it hard for furnace designers to draw fair comparisons between competing grades of candidate refractories. Furthermore, the refractory supplier's data are often not available in a form that can be readily used for furnace design and for the prediction and design of long-term structural integrity of furnace superstructures.

With the aim of providing such comparable data, the US DOE's Office of Industrial Technology and its Advanced Industrial Materials program is sponsoring work to conduct creep testing and analysis on refractories of interest to the glass industry. An earlier stage of the project involved identifying which refractories to test and this is described elsewhere [4]. Conventional silica was one such identified refractory category, and the present report describes the creep behavior of this class of refractories. To portray a more complete understanding of how these refractories perform at service temperatures, their fundamental corrosion resistances, dimensional stabilities, and microstructures were characterized as well.

2. APPROACH

The creep performance of the six refractories was examined. The equipment that was used, the specimen preparation, the employed test matrix, and how the creep data were interpreted are described. The creep results are then presented and compared.

The corrosion resistance of the six refractories was also examined. Like the creep data, the equipment, specimen preparation, test matrix and how the corrosion resistances were interpreted are described. The results are then compared.

The bulk characteristics of the refractories were then characterized before and after their creep testing in an attempt to correlate their changes to the measured creep responses. Bulk density, phase content, microstructure, and secondary phase composition were examined and their changes as a function of test temperature analyzed.

Lastly, the effect of temperature on the dimensional stability of these refractories was examined. Specimens were aged at the same temperatures that the creep tests were performed. The procedures used and the generated results are discussed.

3. MATERIALS AND EXPERIMENTAL PROCEDURES

3.1. MATERIALS TESTED & MANUFACTURER'S REPORTED DATA

Six conventional silica refractories were analyzed in the present study. They were Gen-Sil, SI96AU, Stella GGS, Vega, Vega H, and a yet-unnamed developmental brand manufactured by Harbison-Walker. The manufacturers of these refractories are listed in Table 1.

Table 1. Refractories tested in the present study and their manufacturers.

Refractory Brand Name	Manufacturer
Gen-Sil	A. P. Green
SI96AU	VGT-DYKO
Stella GGS	NARCO
Vega	Harbison-Walker
Vega H	Harbison-Walker
Unnamed Developmental Brand	Harbison-Walker

The manufacturers' reported data regarding some of the chemical, physical and mechanical properties of these refractories were extracted from manufacturers' supplied technical data sheets and summarized in Tables 2 and 3.

All examined brands contained a minimum of 95.5% silica by weight as reported by the manufacturers. The reported chemical constituents, and their amounts, for all brands are listed in Table 2. All brands were "Type A" [5] conventional silicas except SI96AU (a Type B silica refractory); namely, their flux factors (alumina content plus twice the alkali content) were less than 0.50%. The chosen refractories provided a comparison between similar Type A silicas and also between Type A and Type B silicas. According to the published Teltech Report "Crown Refractories for Glass Manufacturing With Oxy-Fuel Combustion" [1], Type B conventional silica is not recommended for use for crowns; however, its mechanical performance at representative furnace crown temperatures and stresses were characterized for the sake of comparison. The major secondary phase constituent in all six brands was calcia (CaO), with additional reported constituents consisting of alumina (Al_2O_3), iron oxide (Fe_2O_3), magnesia (MgO), titania (TiO_2), sodium oxide (Na_2O), and potassium oxide (K_2O). The amounts of these secondary phase

constituents were semi-quantitatively measured by the authors using SEM/EDS and are presented and described in later sections.

Some physical and mechanical properties for these refractories were supplied by the manufacturers, see Table 3. The apparent porosity and bulk density for all six brands were supplied, and respectively ranged between 16.9-25% and 1.75-1.93 g/cm^3. Additionally, changes in dimension due to reheating, hot load testing performance, apparent specific gravity, modulus of rupture, cold crushing strength, and residual quartz contents were also data supplied for some of the six brands. Among the properties listed in Table 3, only the bulk densities of these six brands were measured in the present study along with changes in dimension due to reheating at 1550, 1600, and 1650°C (as a function of time through 250 hours) and may be compared to those values reported by the manufacturers and listed in this table.

Table 2. Refractories manufacturer's reported chemical data.

Constituent	Gen-Sil (%)	SI96AU (%)	Stella GGS (%)	Vega (%)	Vega H (%)	H-W Dev. Brand (%)
SiO_2	95.9	95.5	96.0	96.4	96.1	96.4
Al_2O_3	0.3	1	0.3	0.2	0.4	0.2
Fe_2O_3	0.8	0.3	0.2	0.5	0.6	0.5
CaO	2.8	3	2.6	2.9	2.8	2.9
MgO	0.1	-	-	trace	0.1	trace
TiO_2	trace	0.6	-	trace	0.03	trace
$Na_2O + K_2O$	0.06	0.2	-	0.02	0.03	0.02
Flux Factor*	0.42 Type A	1.4 Type B	0.3 Type A	0.24 Type A	0.46 Type A	0.24 Type A

* Flux factor = Al_2O_3 content + 2 times the total alkali content [5]. A flux factor less than 0.5% denotes a "Type A" silica while "Type B" silica has a value greater than 0.5%.

Table 3. Refractories manufacturer's reported physical and mechanical property data.

Property	Gen-Sil	SI96AU	Stella GGS	Vega	Vega H	H-W Dev. Brand
Reheat change in dimension	-0.1% @ 1600°C			+0.2% @1500°C	+0.1% @1500°C	
Hot Load Test Temp to Failure	1700°C @50psi			1705°C @25psi	1705°C @25psi	1670°C @50psi
Apparent Porosity (%)	21.5	25	21.5	23.3	20	16.9
Apparent Specific Gravity	2.32			2.33	2.32	
Bulk Density (g/cc)	1.82	1.75	1.83	1.79	1.84	1.93
Modulus of Rupture	8.3 MPa 1.2 ksi			6 MPa 0.9 ksi	7 MPa 1 ksi	10.7 MPa 1.55 ksi
Cold Crushing Strength	31 MPa 4.5 ksi	25 MPa 3.6 ksi	40 MPa 5.8 ksi	30 MPa 4.4 ksi	36 MPa 5.2 ksi	
Residual Quartz	< 1%			< 1%	< 1%	

3.2. CREEP TESTING

The creep testing equipment, specimen preparation, the test matrix and testing procedures, and the creep data interpretation method are described.

3.2.1. Equipment

Two testing frames (designated here as CCF1 and CCF2) were used for the compressive creep testing and had some similarities. Both frames consisted of a large clamshell furnace that used resistance-heating, a contacting extensometer that was used to measure axial-dimension-changes, and silicon carbide (SiC) push rods that transferred the applied load from an actuator to the test specimen. The frames had some subtle differences that are described in the detailed descriptions that follow.

Compressive creep frame 1 (CCF1) consisted of a digitally-controlled (LabVIEW™ software, National Instruments, Austin, TX) pneumatic actuator that transferred load to the test specimen through sintered α-SiC (Hexaloy SA™, Carborundum Co., Niagara Falls, NY.) push rods. The push rods were concentrically alignable through translatable adjustments in the load-train's bottom mount. The load train was surrounded by a resistance-heated clamshell furnace (Model 3320, Applied Test Systems, Inc., Butler, PA.) that was capable of heating to 1800°C in ambient air. Within ASTM guidelines [6], temperature fluctuations were approximately ± 2°C and

load fluctuations were less than 1% of test load. Two disposable α-SiC disks (with nominal dimensions of 3mm thickness and 37mm diameter) were inserted in the load train between the test specimen and the α-SiC push rods to prevent chemical reaction between specimen and push rod. The grips that connected the push rods to the test frame or its load cell/actuator were water-cooled using a closed-system water-circulating reservoir. A schematic of CCF1's layout and a picture of its primary components are shown in Figs. 2-3, respectively.

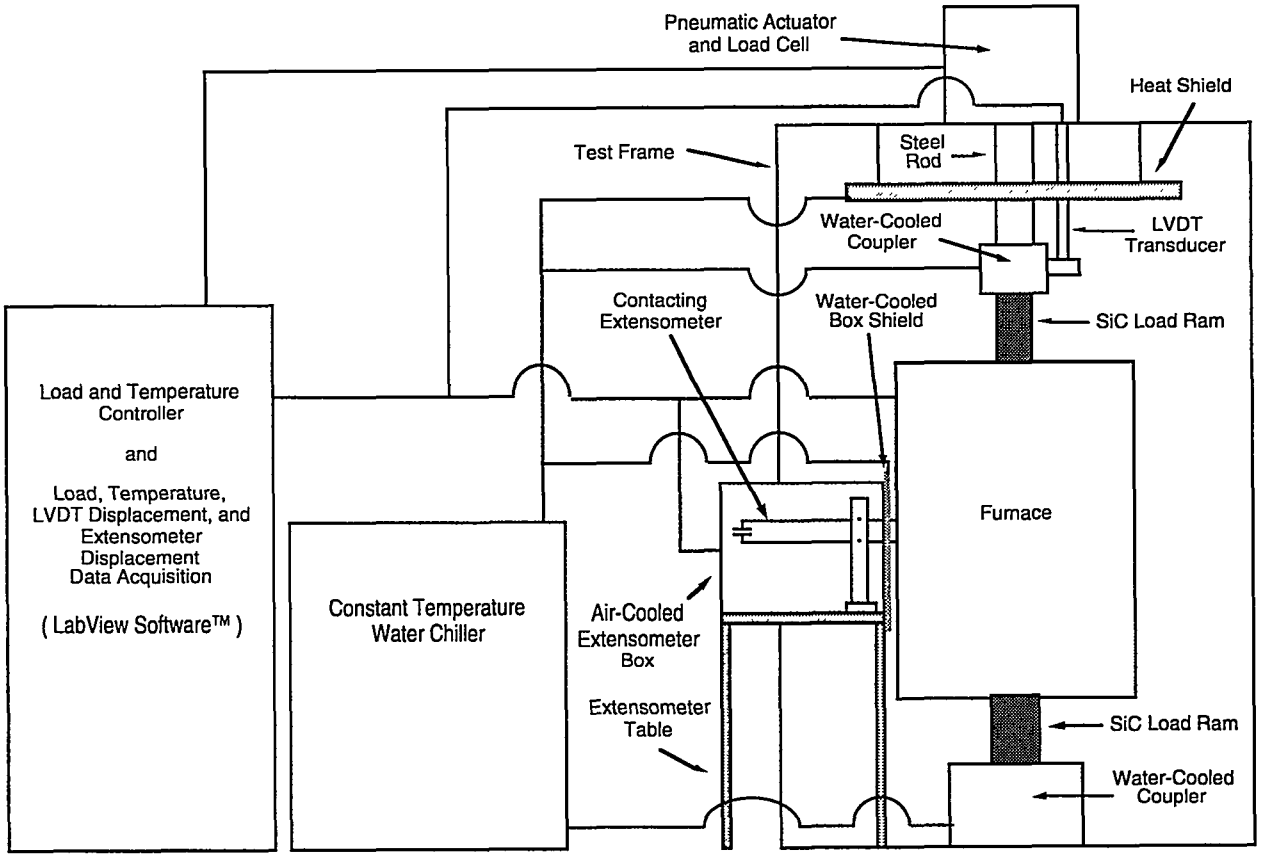

Fig. 2. Schematic of CCF1 and supporting instruments.

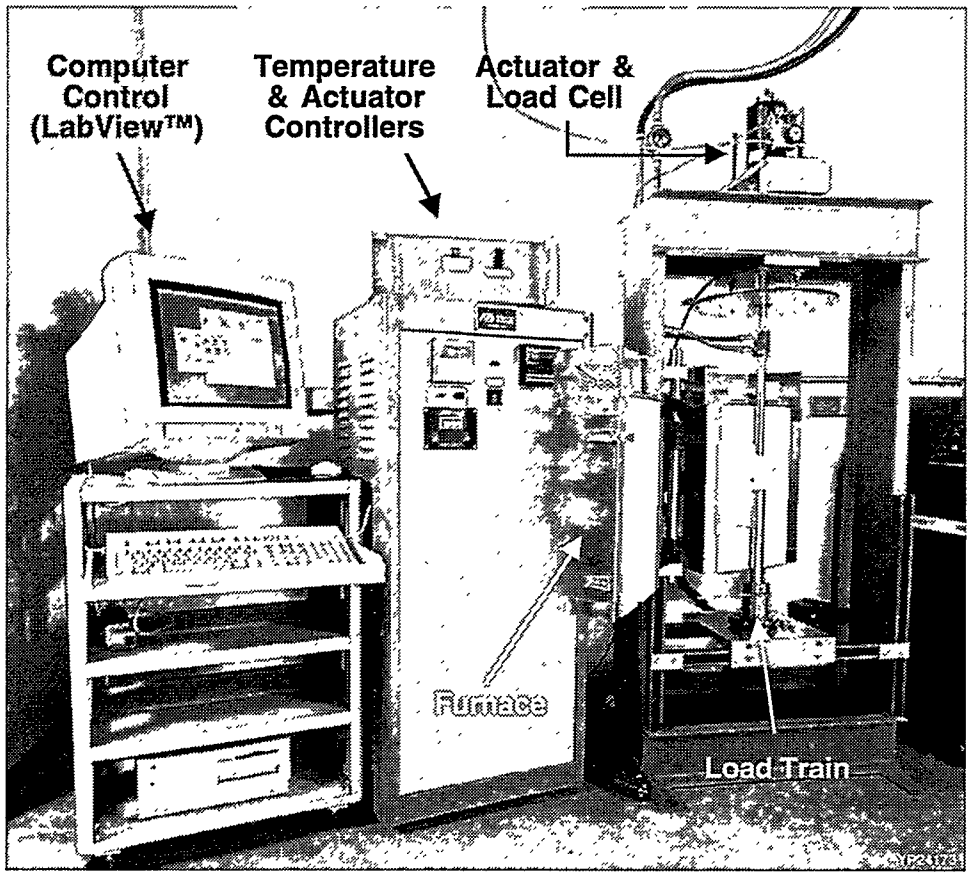

Fig. 3. Primary components of CCF1.

A scissors-type, high-temperature contacting extensometer was used with CCF1 to continuously measure the specimen's axial dimensional change due to the compressive load. The contacting extensometer employed a capacitance sensor whose gap was conditioned and calibrated and measured as a function of time. The extensometer's contacting rods were made of α-SiC. The capacitance gap was correlated with the extensometer's gauge length of 40.00 mm (1.575 inches) and its resolution was approximately 1 μm (0.00004 inches or 0.04 mils) at temperature. A schematic of the CCF1 extensometer layout is shown in Fig. 4.

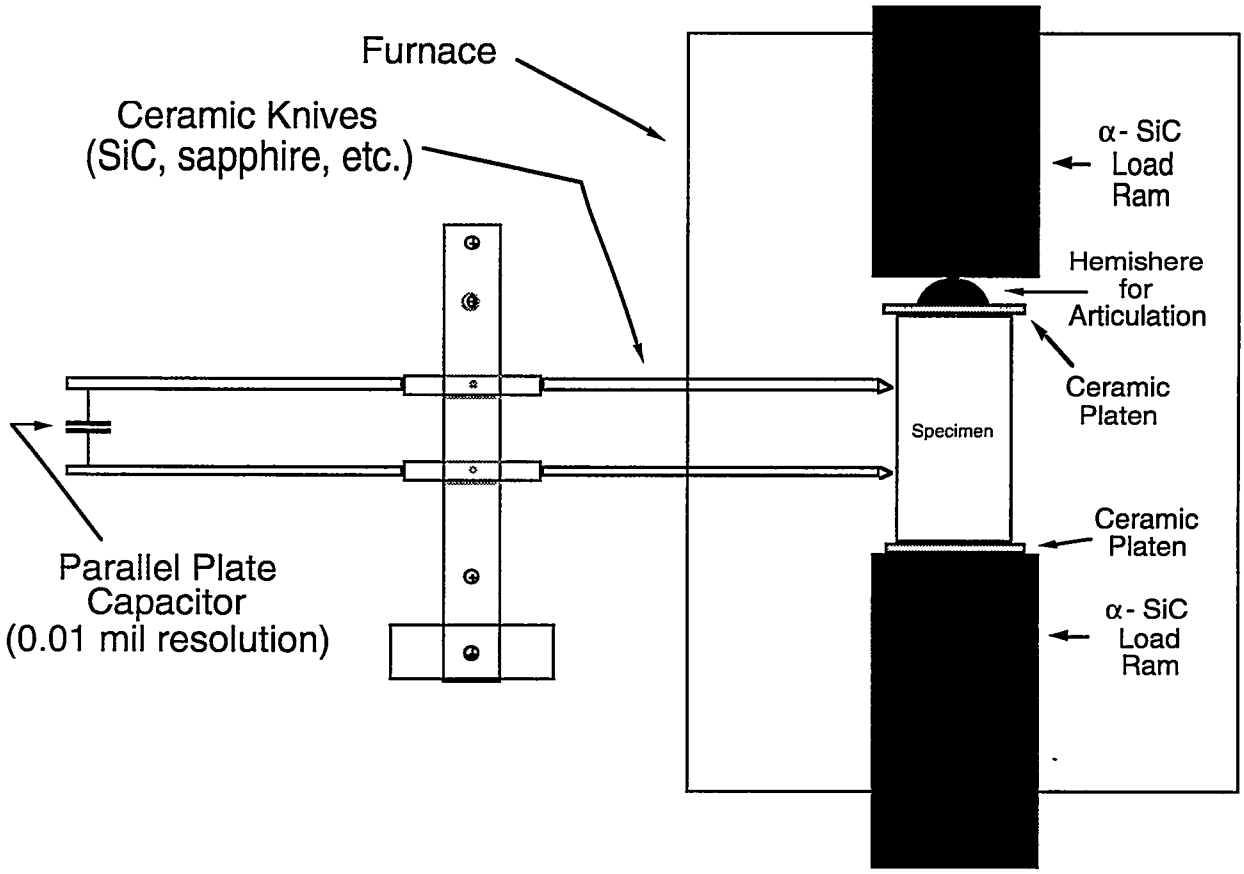

Fig. 4. Schematic of CCF1's extensometer layout.

A schematic and picture of the second creep machine (CCF2) that was used are shown in Figs. 5-6. The system has many similarities to CCF1. Creep tests with CCF2 were accomplished using either pneumatic power digitally controlled by the LabVIEW software or hydraulic power controlled by an analog controller. The latter feature provides both static (creep) and dynamic loading. The test specimen, not visible in Fig. 6, was heated with a high temperature furnace capable of 1800 C (same as CCF1). Within ASTM guidelines [6], temperature fluctuations were approximately ± 2°C and load fluctuations were less than 1% of test load. The specimen was compressed by two long push-rods (each 0.3-m long) with the unheated ends connecting to water-cooled anvils. The upper compression anvil is fixed to the upper platen by a universal joint and leveled using four turnbuckles. The lower compression anvil is resting on a self-aligning coupler which plays an important role in maintaining load-train stability and uniform compression to the specimen. Details of the compressive creep testing system may be found elsewhere [7].

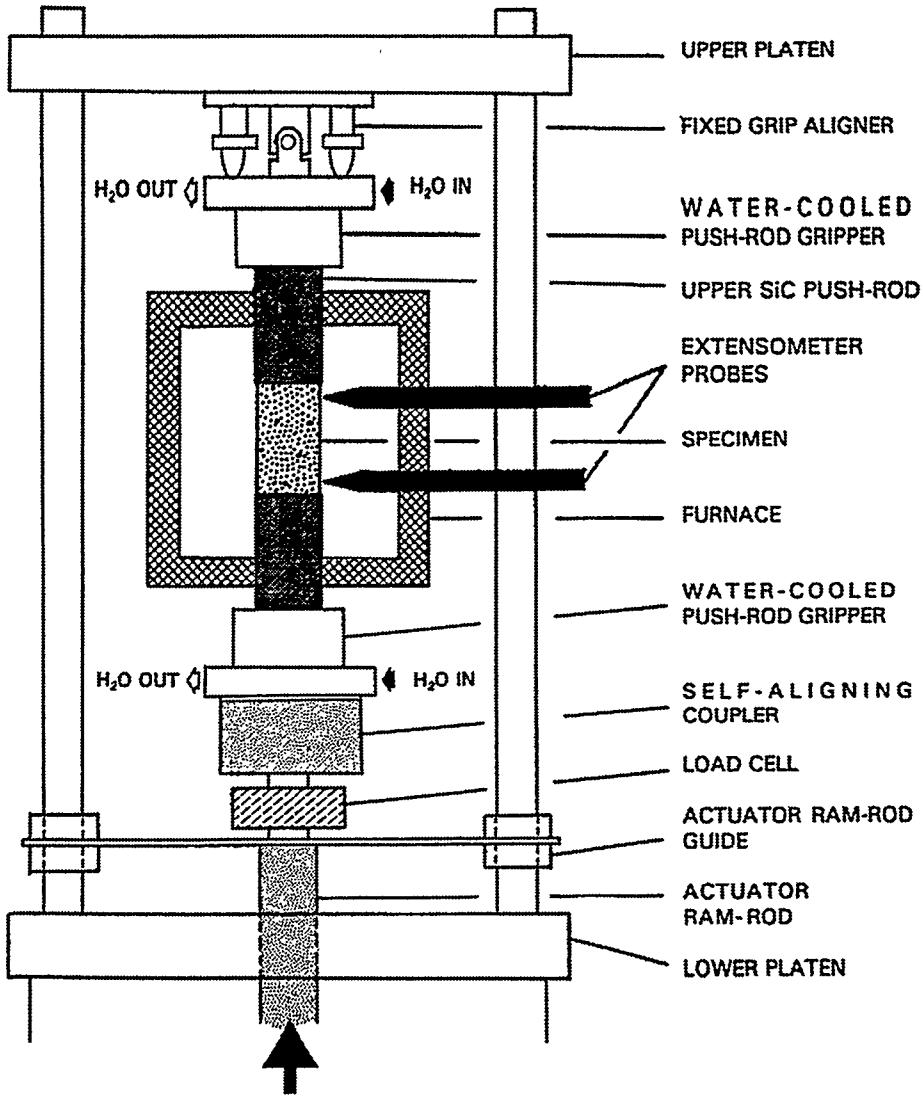

Fig. 5. Schematic of CCF2 and supporting instruments.

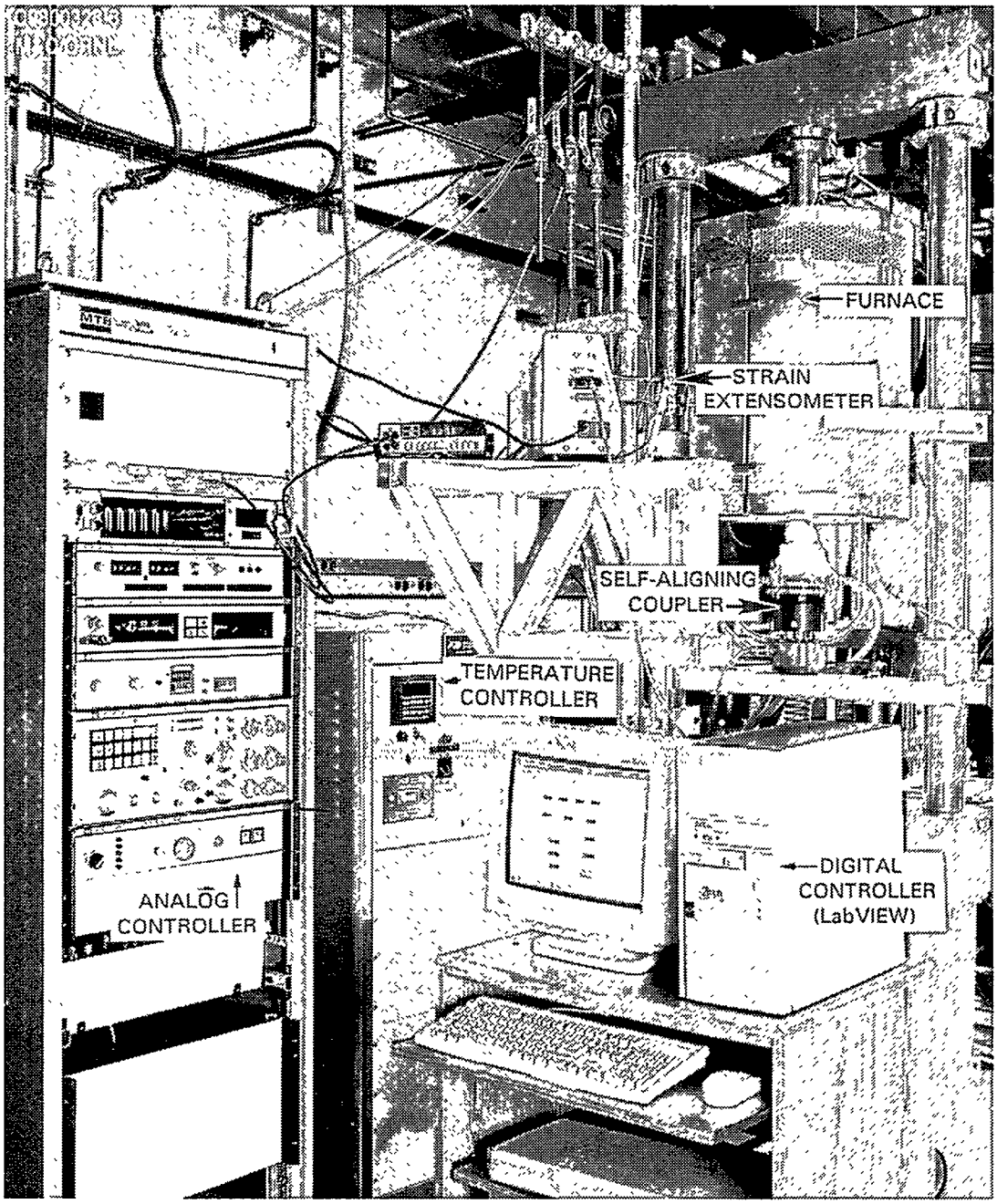

Fig. 6. Primary components of CCF2.

The creep strain generated with CCF2 was measured using a scissors-type mechanical extensometer [8], a schematic of which is shown in Fig. 7. It operates on the same principle as the CCF1 extensometer. The lever-arm assembly was made from a continuous rod of silicon carbide. The probes monitored creep deformation of the specimen continuously in real time with a capacitive transducer attached to the cool end of the extension rod. Concurrently, a laser-based scanner was used to measure the movement of two fiducial flags attached to the ends of the extension rods for verification. The extensometer provided an accuracy and resolution of about 5 μm, which is equivalent to the sensitivity yielded by conventional strain gages. Strain measurements with the transducer and the laser system were in good agreement.

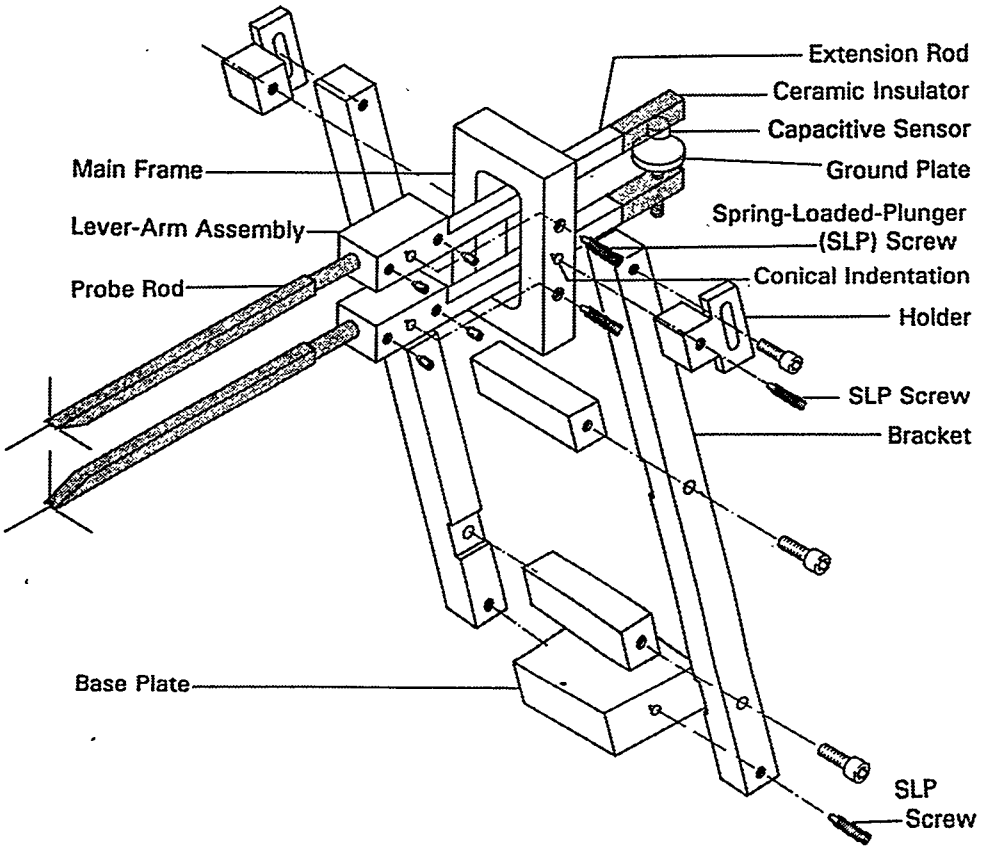

Fig. 7. Schematic of CCF2's extensometer.

The consistency in creep strain measurement between CCF1 and CCF2 were verified prior to the commencement of the test program. Several Gen-Sil test specimens were tested at identical conditions (*i.e.*, same compressive stresses and temperatures for equal times) with each frame consistently yielding statistically equivalent creep strain measurements. With this verified, the authors deemed the measured compressive creep responses of the six silica refractory brands to be independent of which creep frame was used.

Extensometry methods other than the capacitance contacting extensometers used in this study are often used for the measurement of refractory creep; however, the capacitance contacting extensometer circumvents problems that other techniques inherently possess. The deformation of refractories is frequently measured continuously during compressive creep testing using two (sometimes more) linear variable differential transducers (LVDTs) whose mutual displacement coincide with the continuous position of the specimen ends. The creep results generated from this technique are accurate only as long as the accumulated measured deformation coincides with the actual specimen heights measured before and after testing. Deformation and/or translation of the load train during the creep testing of the specimen, reaction of the specimen ends with the fixturing, and "bedding-down" of the specimen all have been shown to cause a lack of correlation between the measured deformation during testing and the change in pre- and post-test specimen height. If any of these events are occurring then the measured contraction during testing is not solely due to creep. Consequently, caution must be exercised when interpreting deformation data generated using this LVDT technique because it will only be representative creep data if the experimenter verified and correlated pre- and post-test specimen height with the accumulated measured deformation. The advantage of the contacting extensometers used in the present study is that their accurate operation is independent of any rigid body motion or deformation of the test hardware, specimen (*e.g.*, "end-crushing"), and push rods.

3.2.2. Specimen Preparation

Cylindrical test specimens were prepared and their dimensions are shown in Fig. 8. They were core drilled from supplied conventional silica bricks in the manner illustrated in Fig. 9. The primary axis of the machined cylinder-shaped specimens was oriented parallel to the pressing direction. Although not verified in the present study, the measured creep deformation was assumed to be isotropic, so specimens were not machined from the silica bricks in different orientations. After core drilling, the specimen ends were ground parallel to within 0.013 mm (0.001 inches). All specimens were dried in an oven at 300°C (570°F) for 4 hours after they were core drilled and before they were creep tested.

Using an appropriate aspect ratio of compression test specimens is an important consideration. A specimen aspect ratio of 2.6 or greater is recommended for *compressive strength tests* so that the friction effects between the specimen ends and loading ram are small compared to the axially applied compressive stresses [9]. However, in the present study (aspect ratio = 2.0), the applied axial compressive stresses during creep testing were already low (*i.e.*, much less than the refractories' compressive strengths). Consequently, the stresses and strains due to such friction were likely negligible, so adherence to the height/diameter ratio of 2.6 or greater was deemed unnecessary.

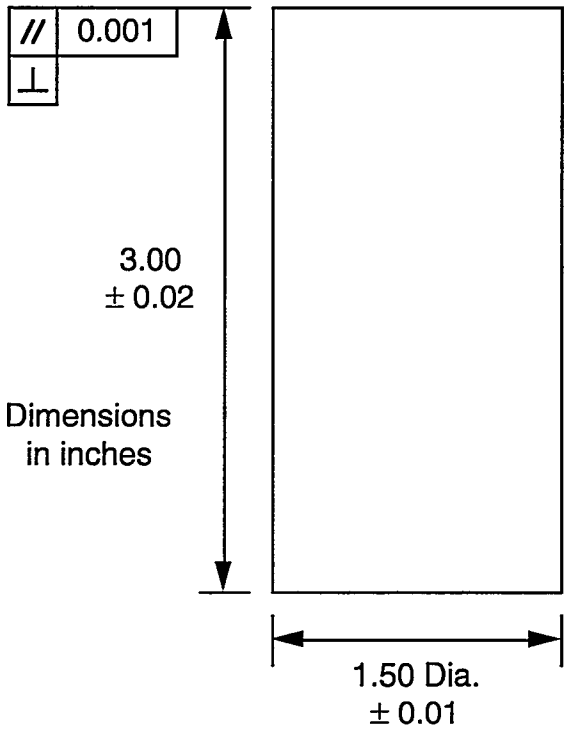

Fig. 8. Dimensions of core-drilled test specimens.

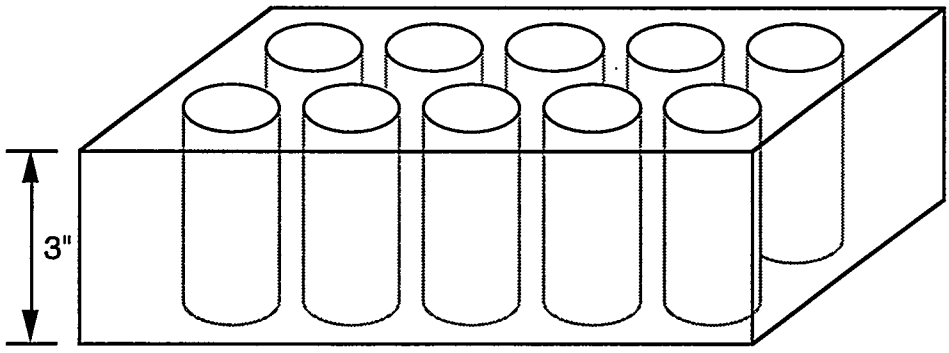

Fig. 9. Schematic of how specimens were core-drilled from as-received bricks.

3.2.3. Test Matrix & Procedure

A total of 18 specimens was tested (three stresses per specimen), and the test matrix is shown in Table 4. One specimen from each of the six brands was tested at 1550°C (2820°F), 1600°C (2910°F), and 1650°C (3000°F). Repeatability in the creep performances of the silica materials was not examined with the exception of Gen-Sil silica. As described, duplicate Gen-Sil specimens were used for the initial creep frame consistency and comparison analyses, and were found to equivalently creep at the same test conditions.

The applied stress and temperature histories are illustrated in Fig. 10. All specimens were preloaded in compression to approximately 0.04 MPa (≈ 6 psi) during furnace heatup to keep all the load train components and specimen in continuous contact. The specimens were heated from room temperature to the test temperature in 4 hours. Each of the specimens was soaked at temperature for 25 hours prior to the application of the first stress. All specimens were loaded sequentially at three stresses: 0.2, 0.4, and 0.6 MPa (29, 58, and 87 psi) for 75 hours at each level. Creep strain was measured as a function of stress, time, and temperature using the described extensometers and computer data acquisition.

Table 4. Test matrix for creep testing.

Refractory	1550°C (2820°F)	1600°C (2910°F)	1650°C (3000°F)
Gen-Sil	0.2, 0.4, & 0.6 MPa (29, 58, & 87 psi)	0.2, 0.4, & 0.6 MPa (29, 58, & 87 psi)	0.2, 0.4, & 0.6 MPa (29, 58, & 87 psi)
SI96AU	0.2, 0.4, & 0.6 MPa (29, 58, & 87 psi)	0.2, 0.4, & 0.6 MPa (29, 58, & 87 psi)	*
Stella GGS	0.2, 0.4, & 0.6 MPa (29, 58, & 87 psi)	0.2, 0.4, & 0.6 MPa (29, 58, & 87 psi)	0.2, 0.4, & 0.6 MPa (29, 58, & 87 psi)
Vega	0.2, 0.4, & 0.6 MPa (29, 58, & 87 psi)	0.2, 0.4, & 0.6 MPa (29, 58, & 87 psi)	0.2, 0.4, & 0.6 MPa (29, 58, & 87 psi)
Vega H	0.2, 0.4, & 0.6 MPa (29, 58, & 87 psi)	0.2, 0.4, & 0.6 MPa (29, 58, & 87 psi)	0.2, 0.4, & 0.6 MPa (29, 58, & 87 psi)
Unnamed Development Brand	0.2, 0.4, & 0.6 MPa (29, 58, & 87 psi)	0.2, 0.4, & 0.6 MPa (29, 58, & 87 psi)	0.2, 0.4, & 0.6 MPa (29, 58, & 87 psi)

* This material exhibited excessive creep deformation at 1600°C, so its testing at 1650°C was omitted.

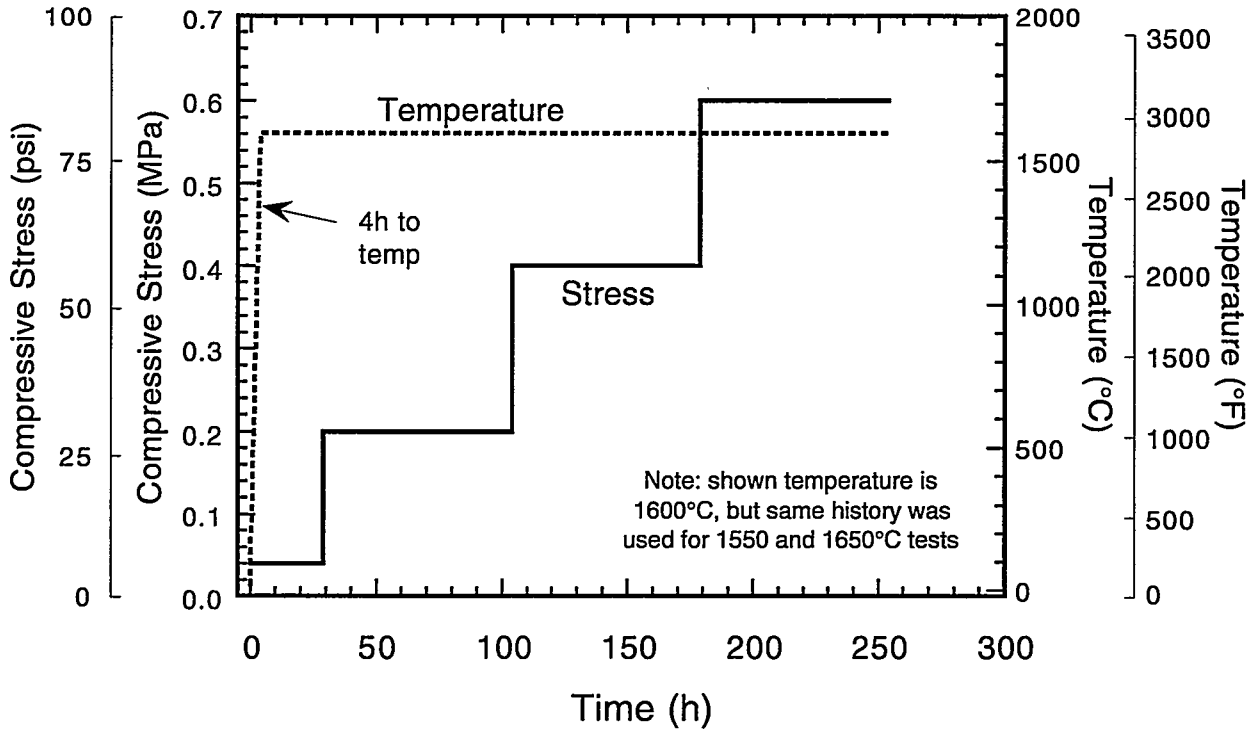

Fig. 10. Temperature and stress history used in the creep testing.

There are load testing protocols for refractories [6, 10], but they were not strictly adhered to for reasons that follow. The testing procedure used in the present study either circumvents some of the shortcomings of those tests, or it involves the testing of more creep resistant refractory materials at higher temperatures. The "Standard Test Method for Load Testing Refractory Brick at High Temperatures" [10] involves loading a refractory brick for a prescribed duration and temperature and then determining the material's resistance to deformation by comparing its before- and after-test axial dimension. A shortcoming of this test is the introduction of error in the analysis if the refractory brick's ends "bed-down." The procedures and equipment recommended in the "Standard Test Method of Measuring the Thermal Expansion and Creep of Refractories Under Load" are similar to those used in the present study. A shortcoming of this procedure involves the recommended measurement of dimensional change in the creep specimen. The use of LVDTs to measure the contraction of the specimen ends is advocated and can be problematic for reasons described in Section 3.2.1. The extensometry system described in Fig. 2 of ASTM C832 [6] closely matches the extensometry system used in the present study; however, that in the present study uses a capacitance gage while that in the standard shows the use of a LVDT for the measurement. The load that activates an LVDT can be enough to affect the intimacy of the extensometer contact with the specimen and yield a misleading creep measurement if there is

insufficient horizontal load applied to the specimen. Because of its differing operating principle, the capacitance gage on the extensometry systems used in the present study requires no load for activation and does not introduce uncertainties associated with the horizontal load and the use of a LVDT.

3.2.4. Data Interpretation

Most creep analyses for long-term applications (*i.e.*, where steady state creep accumulation dominates the accumulation of strain, not the amount of primary creep) involve the determination of a steady-state or minimum creep rate and its examination as a function of applied stress and temperature. The steady-state or minimum compressive creep rate ($d\varepsilon/dt_{min}$) can be related to the applied compressive stress and temperature using an empirical Arrhenius power law or the familiar Norton-Bailey creep equation [11]:

$$d\varepsilon/dt_{min} = A\,\sigma^{n} \exp(-Q/RT), \qquad [1]$$

where A is a constant, σ is the applied stress, n is the stress exponent, Q is the activation energy, R is the gas constant, and T is the absolute temperature. Multilinear regression may be performed to determine the constants A, n, and Q for each material. By performing the analysis in this manner, it is implied the same dominant (or rate-controlling) creep mechanism is active at all temperatures and stresses. The validity of this assumption is assessed by the goodness-of-fit of this equation to the experimental data and the reasonableness of the obtained values for n and Q.

An example of this analysis is demonstrated using compressive creep data of a MgO refractory [12]. Compressive creep strain as a function of stress and time is shown in Fig. 11 for a 96.1% MgO refractory tested at 1550°C (2820°F) that is used as checker packing in furnace regenerators. The steady-state or minimum creep rate is then determined and related to the applied stress and temperature. If more than one temperature is used for the creep tests, then these creep rate data may be applied to Eq. 1 (see Fig. 12). Such data may then be used by superstructure designers to calculate (interpolate) any creep rate as a function of stress and temperature: this allows for superstructure design optimization and its prediction of mechanical integrity. A goal of the present study was to determine such creep rate data for each examined silica refractory.

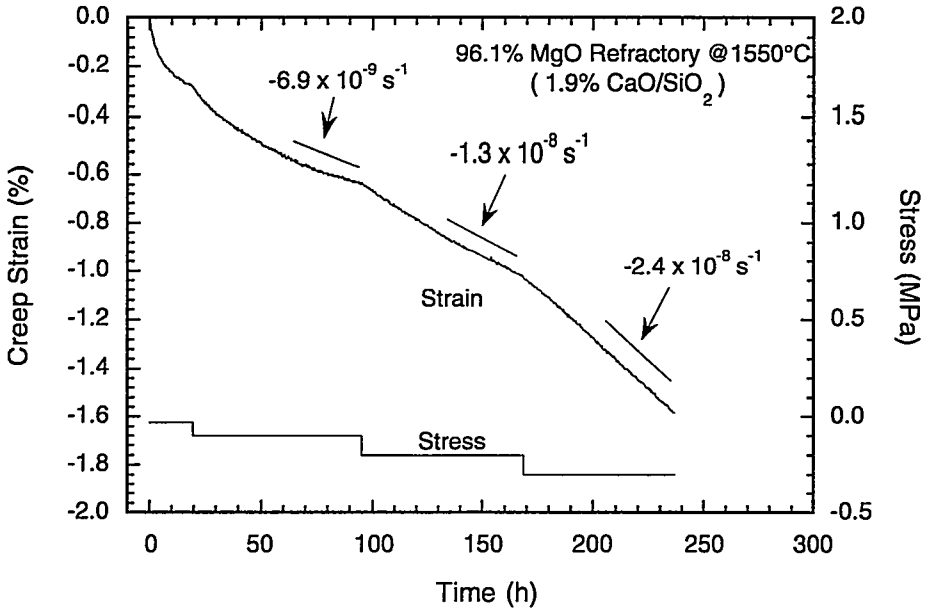

Fig. 11. Example of a compressive creep curve (creep strain as a function of stress and time) and the determinations of creep rate [12].

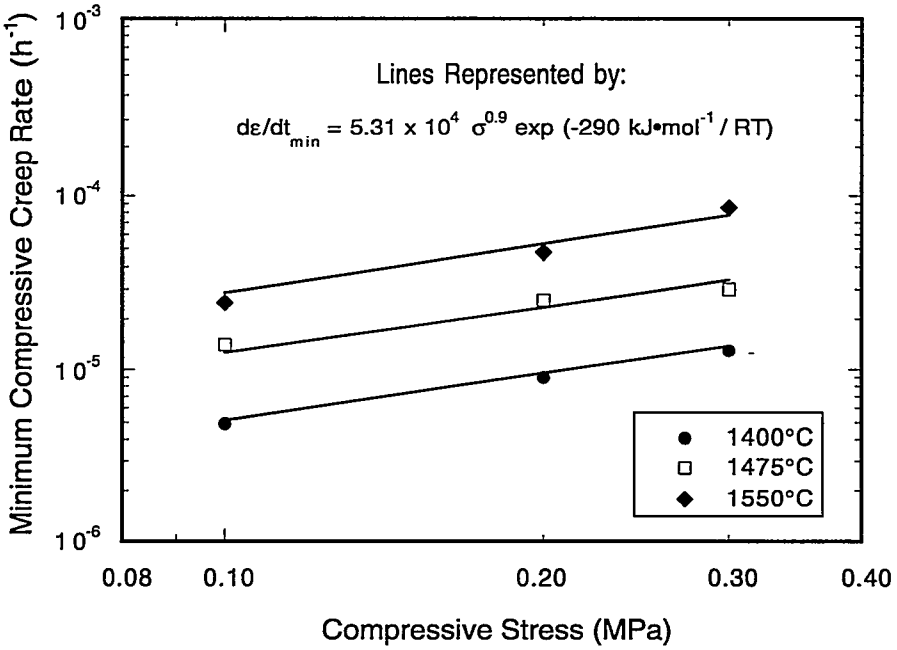

Fig. 12. Example of an empirical power-law representation (Eq. 1) of creep rate as a function of stress and temperature.

3.3. CORROSION TESTING

Corrosion rates were measured on the six silica refractories using the ASTM "lid test" [13]. A refractory specimen (2.5cm x 2.5cm x 1cm) sectioned from the as-received silica bricks was placed over a small alumina crucible containing 12.5g of sodium carbonate. The crucible and "lid" refractory specimen were then placed in a secondary alumina container and isothermally exposed at 1400°C for 24h.

In order to further assess the parameters of the ASTM lid test, two variables were explored in a supplemental study; temperature and the amount of sodium carbonate. This specific analysis was only performed using one refractory (Gen-Sil) because the emphasis was on the two mentioned independent parameters, not to compare their effects with all six silicas.

3.4. BULK CHARACTERISTICS (PRE- AND POST-CREEP-TESTING)

Supplemental efforts were performed to characterize some physical and chemical properties of the silica refractories. The bulk density, phase content, microstructure (as exploited by reflected light and cathodoluminescence imaging), and secondary phase composition of each silica brand before and after testing were measured or characterized. Bulk density, volume, and weight changes due to temperature exposure were additionally examined (in the absence of stress) with each of the six silica refractories.

3.4.1 Bulk Densities

The bulk densities of the core drilled specimens were measured prior to their creep testing. Their masses were measured using a balance that had a resolution of $\pm$ 0.0005 g. The masses were then divided by the respective specimens' volumes (diameters and lengths measured with calipers having a resolution of $\pm$ 0.005 mm) to calculate density. Each silica brick yielded 10 specimens, so the average bulk density for each brick was calculated using these 10 values.

The bulk densities of crept specimens were also measured and compared to those of their "as-received" state. It was found that specimens did not substantially compressively creep so "barreling" did not occur in them with the exception of SI96AU tested at 1600°C. Consequently, the bulk density of those specimens that did not "barrel" were measured in the same manner as the "as-received" specimens. Because the SI96AU specimen substantially crept, it no longer maintained a cylinder geometry so it was coated with paraffin wax and its density was measured using the water immersion technique via ASTM C914 [14].

3.4.2. Crystalline Phases

The phase content of the materials' "as-received" state was characterized and compared with that after creep testing at 1550, 1600, and 1650°C. Specimen preparation involved grinding the silica refractory to approximately 325 mesh in an agate mortar and pestle.

X-ray diffraction (XRD) was performed with all six silica materials using a Scintag 2000 diffractometer. The samples were scanned at a rate of 1°/min with Cu Kα radiation (λ = 1.54059Å), and a step size of 0.02° over a scan range of 10 to 120° two-theta.

A Pearson III profile fitting function was applied to the strongest diffraction lines of cristobalite (2θ=21.989°) and tridymite (2θ=21.765°) to estimate the relative ratio of cristobalite to tridymite for each of the six brands (a comparison of peak areas), and to also make qualitative assessments of how much of each phase was present in the materials and to examine how their contents changed as a consequence of the creep testing.

3.4.3. Microstructures

Disks were sectioned from core-drilled "as-received" specimens, as well as from crept specimens, in preparation for reflected light (RL) and cathodoluminescence (CL) imaging. A disk was cut from the top of one of the untested core-drilled specimens from each of the silica refractories as shown in Fig. 13. Disks were sectioned from crept specimens in their centers as shown in Fig. 14.

The disk sections were polished using the following procedures in preparation for the microscopy. The disks were cleaned, dried and then impregnated with a low viscosity resin to fill the pores. The impregnated specimens were then mounted on a Co-Cast mounting media. Cured sections were ground with diamond wheels down to 600 grit, and then finally polished with diamond paste and lapping oil.

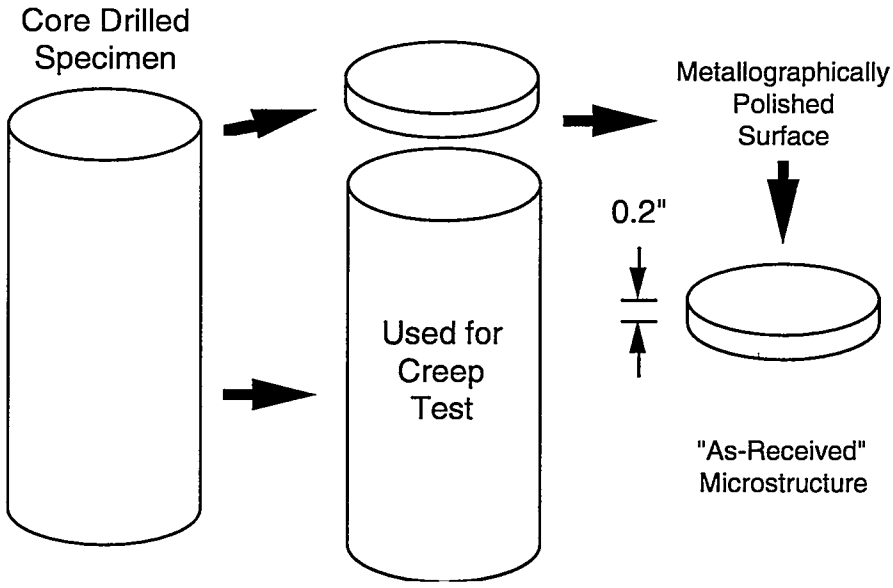

Fig. 13. Schematic describing how disk sections were machined from core drilled specimens for "as-received" RL and CL imaging.

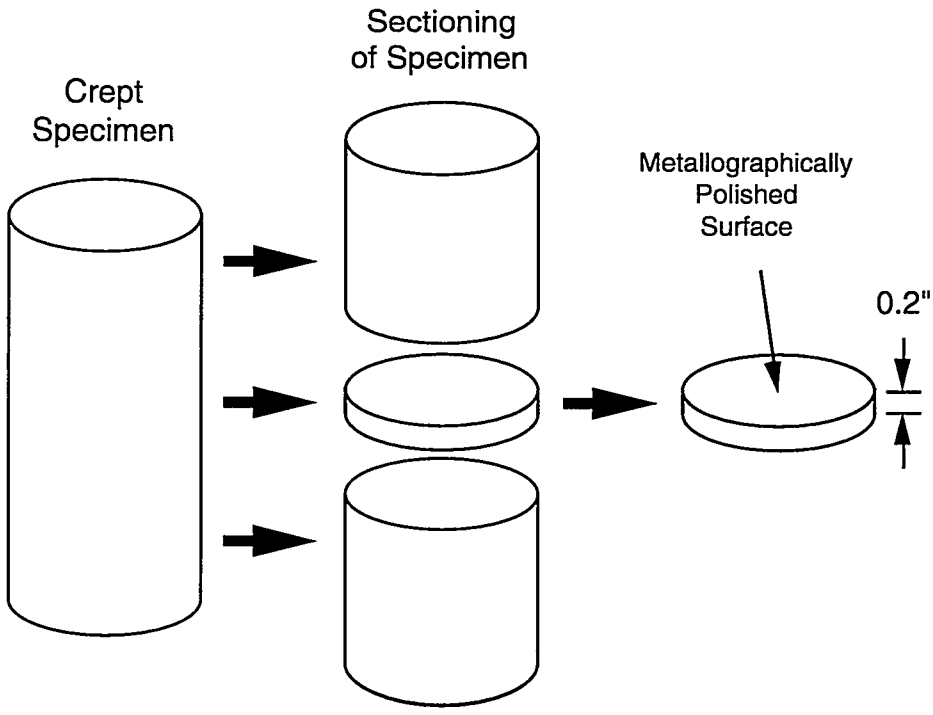

Fig. 14. Schematic describing how disk sections were machined from crept specimens for post-testing RL and CL imaging.

Reflected light and CL microscopy were utilized for the characterization. A cold-cathode CL microscopy system (Model Mk4, Cambridge Imaging Technology, Cambridge, UK) mounted on a standard Nikon petrographic microscope (Model Labophot-Pol with a Nikon UFX-DX photomicrographic system) was used for these microstructural analyses.

The CL microscopy characterization technique has been described in detail by Karakus and Moore [15], but is briefly described here. The CL imaging system utilizes an energetic electron beam that is produced from a cold cathode ray tube. The electron beam is trained on the surface of uncovered polished or unpolished specimens in a low vacuum environment. As a result of the electron beam-solid specimen interaction, minerals or phases in the specimen produce characteristic colored light known as "cathodoluminescence" emission. The CL technique is unique and provides microstructural information that often cannot be obtained by any other technique. The CL microscopy system can provide immediate assessment of the phases in refractory materials through the identification of characteristic CL color and crystal habits that minerals exhibit. The CL microscopy system can also be used in conjunction with RL and SEM for elemental analysis of individual phases.

Certain minerals produce characteristic CL color. For example, corundum (α-Al_2O_3) is characterized by a characteristic bright red CL color while spinel ($MgAl_2O_4$) produces a characteristic green color. These CL emissions are due to "activator" elements present in trace amounts in these mineral structures; Cr^{3+} in corundum produces a characteristic CL emission at approximately 694 nm and tetrahedrally coordinated Mn^{2+} in spinel produces a CL emission at approximately 520 nm. Activator elements related to CL emission centers in these minerals often require low voltages ($\approx$ 8kV) for excitation.

Silica minerals, including quartz, cristobalite, tridymite, and fused silica, are interesting because they can change their CL color and intensity over time. Unlike corundum and spinel, these silica minerals require relatively high excitation voltages. The CL phenomenon in silica minerals is known to be due to intrinsic defects. Although the CL in silica minerals is not completely understood, they are known to exhibit red, dull blue, yellow, and brown CL color in natural rocks depending on their geochemical environments. Quartz sand in refractories and slags mostly exhibits bright-red (650 nm) and blue (450 nm) CL colors. Cristobalite, tridymite, and fused silica in refractory ceramics exclusively exhibit intense blue CL in varying intensities, with the former two of primary interest to the present study.

3.4.4. SEM/EDS

Scanning electron microscopy (SEM) with electron dispersive spectroscopy (EDS) were used to characterize the grain boundary (secondary) phase in the six crept silica refractories tested at 1600°C. A JEOL T330 SEM with a Kevex EDS system was used.

3.5 EFFECT OF TEMPERATURE ("AGING" STUDY)

To examine dimensional stability due entirely to exposure to temperature, three prismatic bars from each silica refractory (18 total specimens) were prepared and one each subjected to 1550, 1600, or 1650°C for equivalent times to those that the creep specimens were subjected to. Dimensions of these bars are shown in Fig. 15. The 2 in. length of the specimen was parallel to the bricks' pressing direction. These specimens were dried in an oven at 300°C (570°F) for 4 hours after they were machined and before they were aged. The aging procedure consisted of the following: six specimens (one of each material) were heated to one of the three setpoint temperatures in 4 hours; they were soaked at temperature for 25 hours; the furnace was then cooled to ambient; specimens were removed, weighed and their dimensions measured; specimens were put back in the furnace and the procedure was repeated for 100, 175, and 250 cumulative hours. The mass, dimensions (volume), and density of the bars were measured and analyzed as a function of cumulative time and temperature.

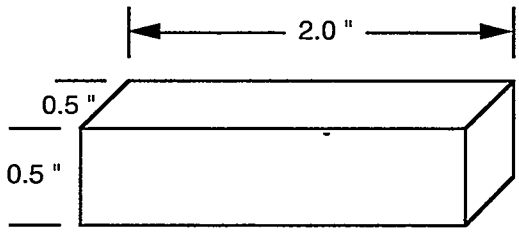

Fig. 15. Schematic of specimens used for the "aging" study.

It is not known if the creep deformation, expansion phenomena, loss in mass, or decrease in density for these six silica brands were a function of specimen size. The reader is urged to interpret the above such mentioned data with caution, and asked to be cognizant of the specimen sizes and geometries used and the results that they produced. There is no known information to suggest that these phenomena are a function of specimen size; however, there is also no known information to

indicate that these properties are independent of size. Additionally, the aging specimen tests were interrupted to measure their dimensions and to weigh them; it is not known if the additional cooling and heating segments affected the accumulated changes in dimension and mass.

4. RESULTS AND DISCUSSION

4.1. COMPRESSIVE CREEP PERFORMANCE

The amount of compressive creep of Gen-Sil, Stella GGS, Vega, Vega H, and Harbison-Walker's new developmental brand conventional silica was negligible at temperatures between 1550-1650°C (2820-3000°F) and at compressive stresses between 0.2 to 0.6 MPa (29-57 psi), see Figs. 16-20. Only one specimen per condition was tested so the authors were unable to statistically conclude that any one of these five brands had superior creep resistance to the others; if differences do indeed exist, then they are believed to be insignificant.

The compressive creep of SI96AU (Type B silica) conventional silica was negligible at 1550°C (see Fig. 21); however, its creep resistance was found to be much less than the other five conventional silicas (which are Type A silicas) at 1600°C (note the differences in creep strain scaling in the two graphs in Fig. 21). SI96AU was not creep tested at 1650°C; however, its creep deformation was anticipated to be inferior to the other five silica brands.

Concurrently active mechanism(s), other than creep, resulted in larger (or oppositely anticipated) dimensional changes than were produced by creep; this effect limited the ability to identify or interpret the lesser-active creep mechanism in these silica refractories. Consequently, the compressive creep rates of all six brands were not able to be represented as a function of temperature and compressive stress using the conventionally used Arrhenius Norton-Bailey creep equation (*i.e.*, the Arrhenius power-law creep model). Multilinear regression of Eq. 1 using the indicated creep rates as a function of stress and temperature yielded undefined values for the constants in that equation. Unlike the creep behavior illustrated for the MgO refractory in Fig. 11, the apparent creep rates were inconsistent in that they were positive-valued (indicative of axial expansion) or were negative-valued (indicative of axial contraction). New models or models other than the Norton-Bailey model (or equivalent "creep" models that represent creep rate as a function of temperature and stress) should be used to represent or predict the long-term dimensional instability of conventional silica superstructures that are subjected to compressive stresses less than 0.6 MPa and temperatures between 1550 and 1650°C.

Some specimens exhibited axial expansion during creep testing even though an axial compressive load was applied. This peculiarity is a consequence of the bulk expansion that these refractories exhibited. This phenomenon is further described in the next sections.

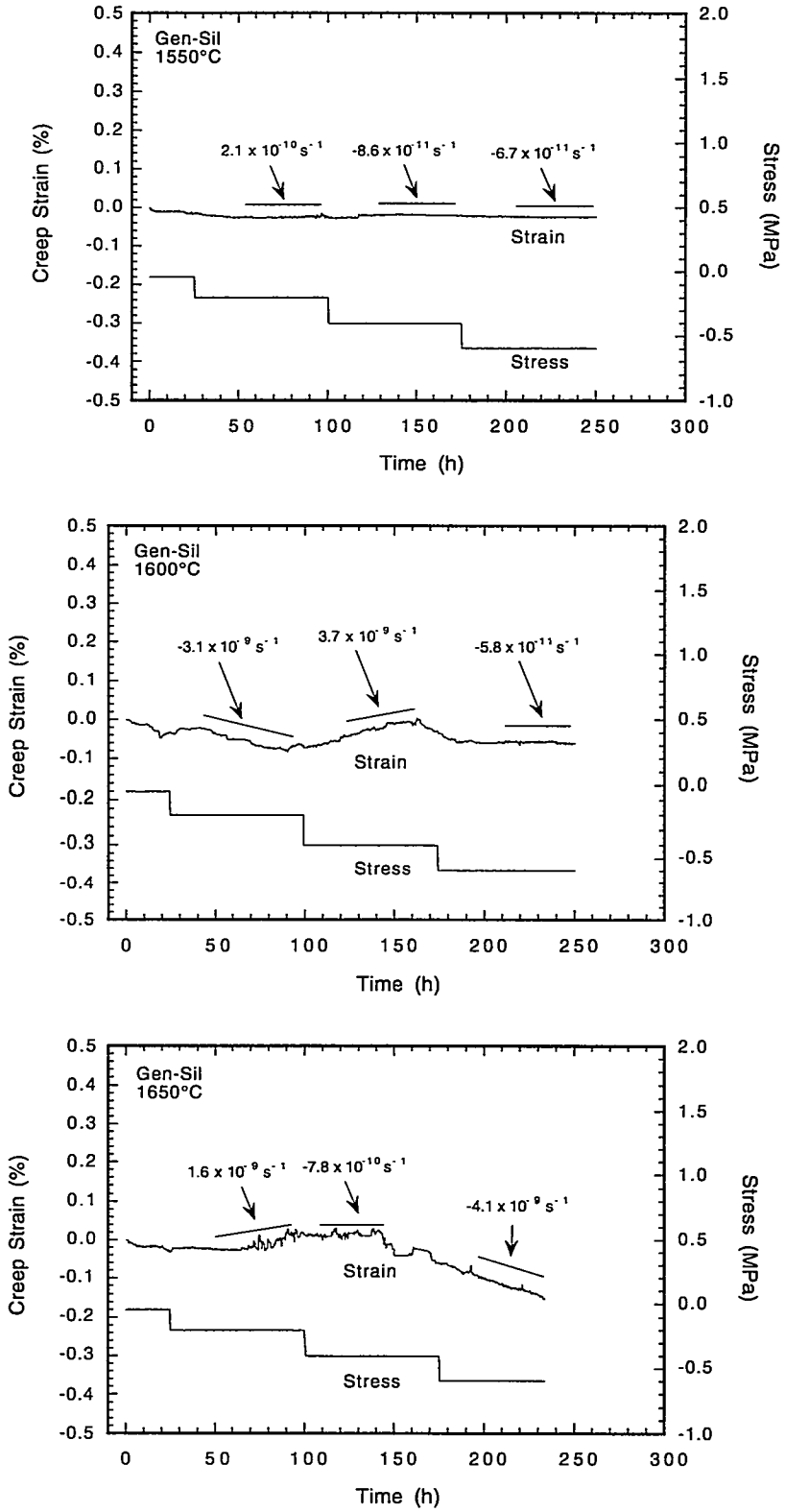

Fig. 16. Creep behavior of Gen-Sil as a function of temperature.

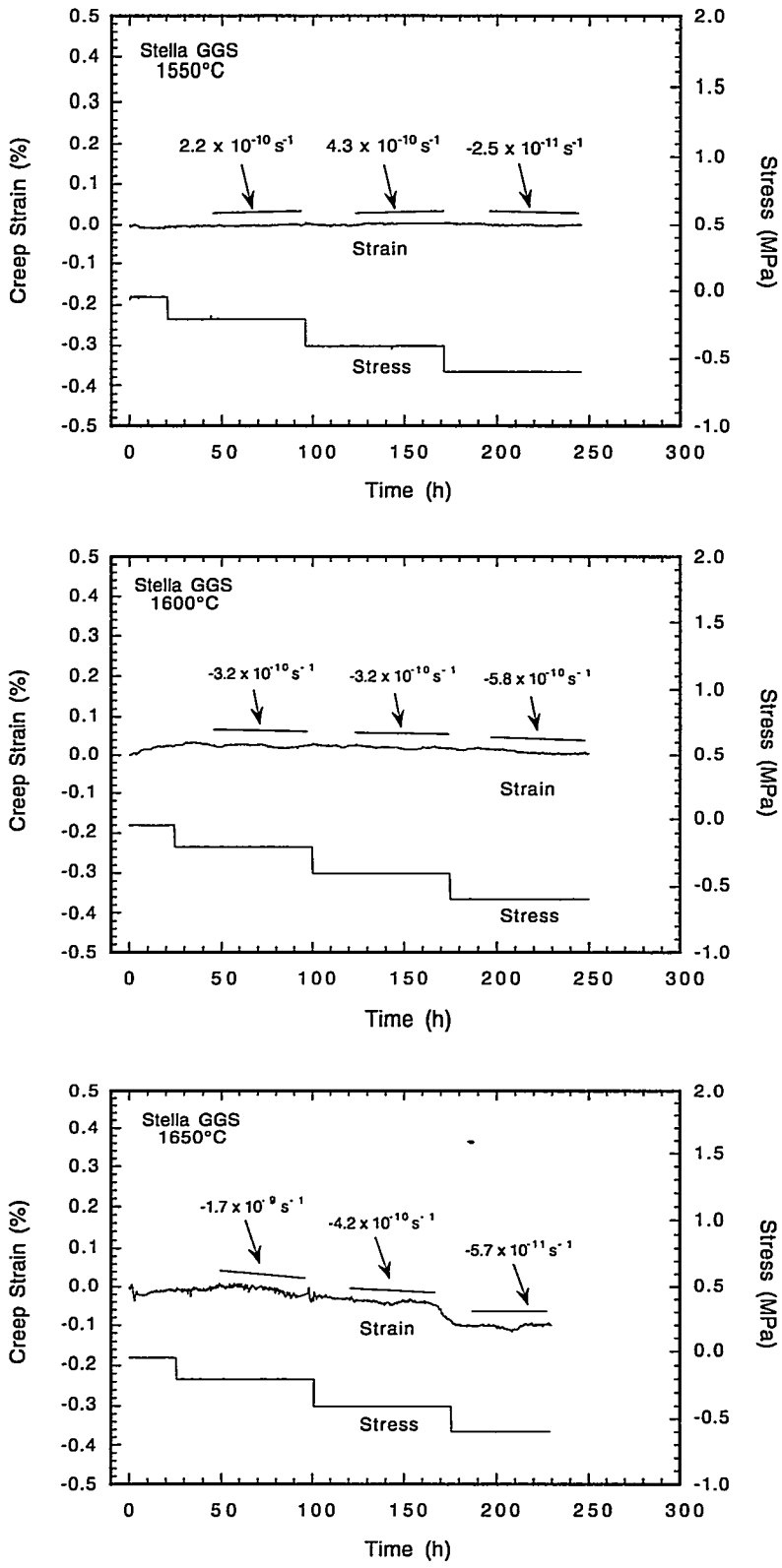

Fig. 17. Creep behavior of Stella GGS as a function of temperature.

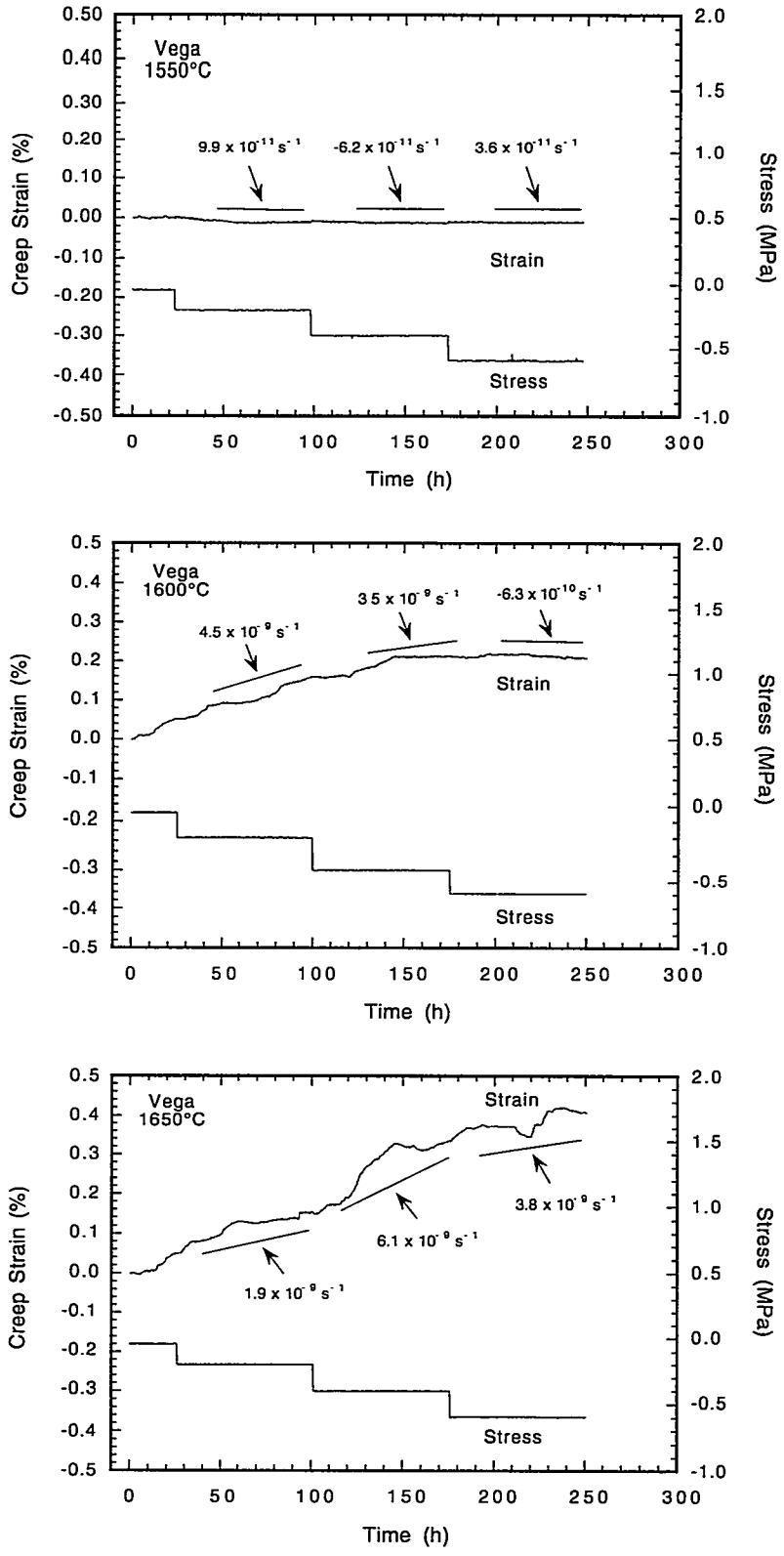

Fig. 18. Creep behavior of Vega as a function of temperature.

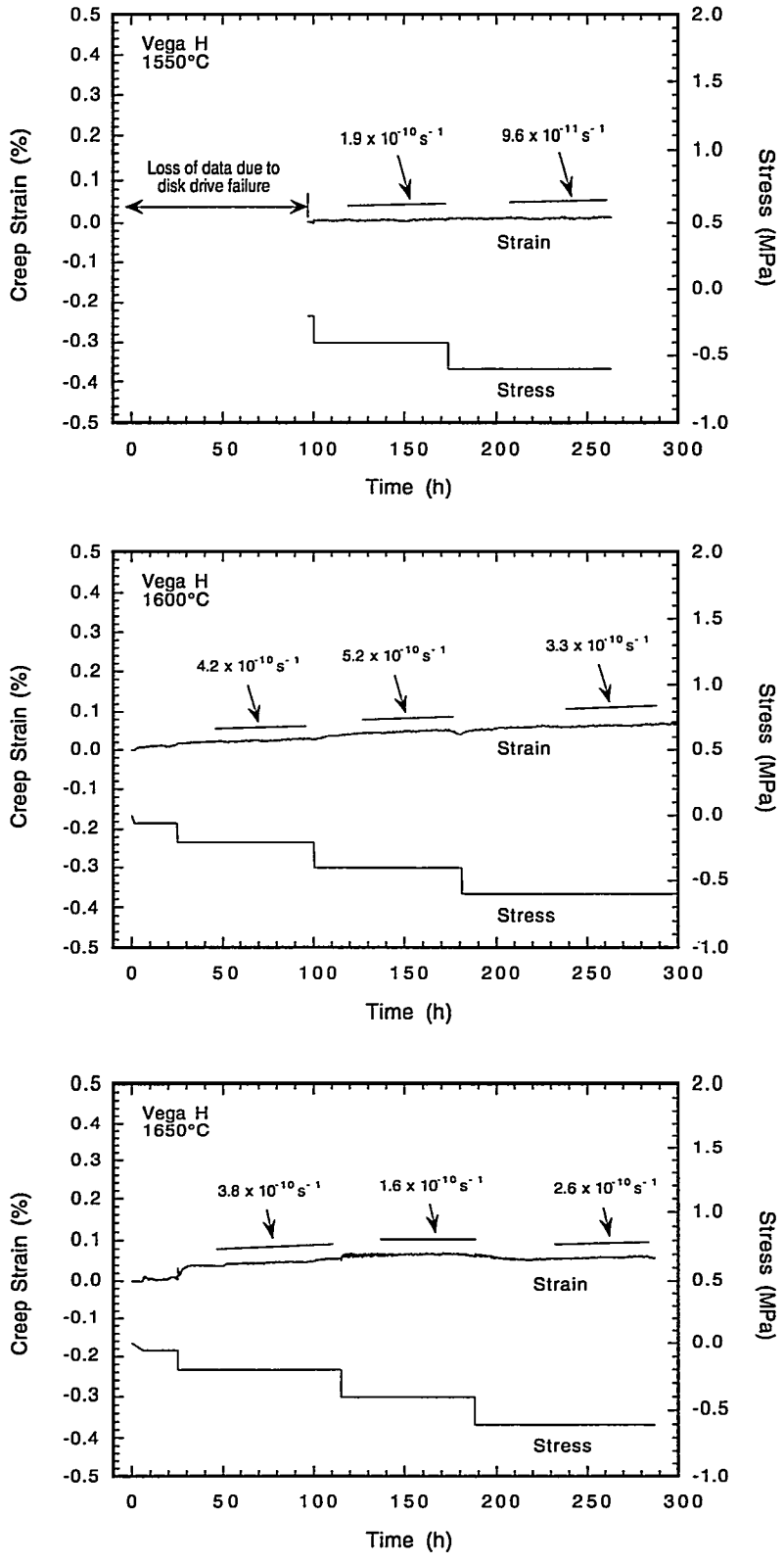

Fig. 19. Creep behavior of Vega H as a function of temperature.

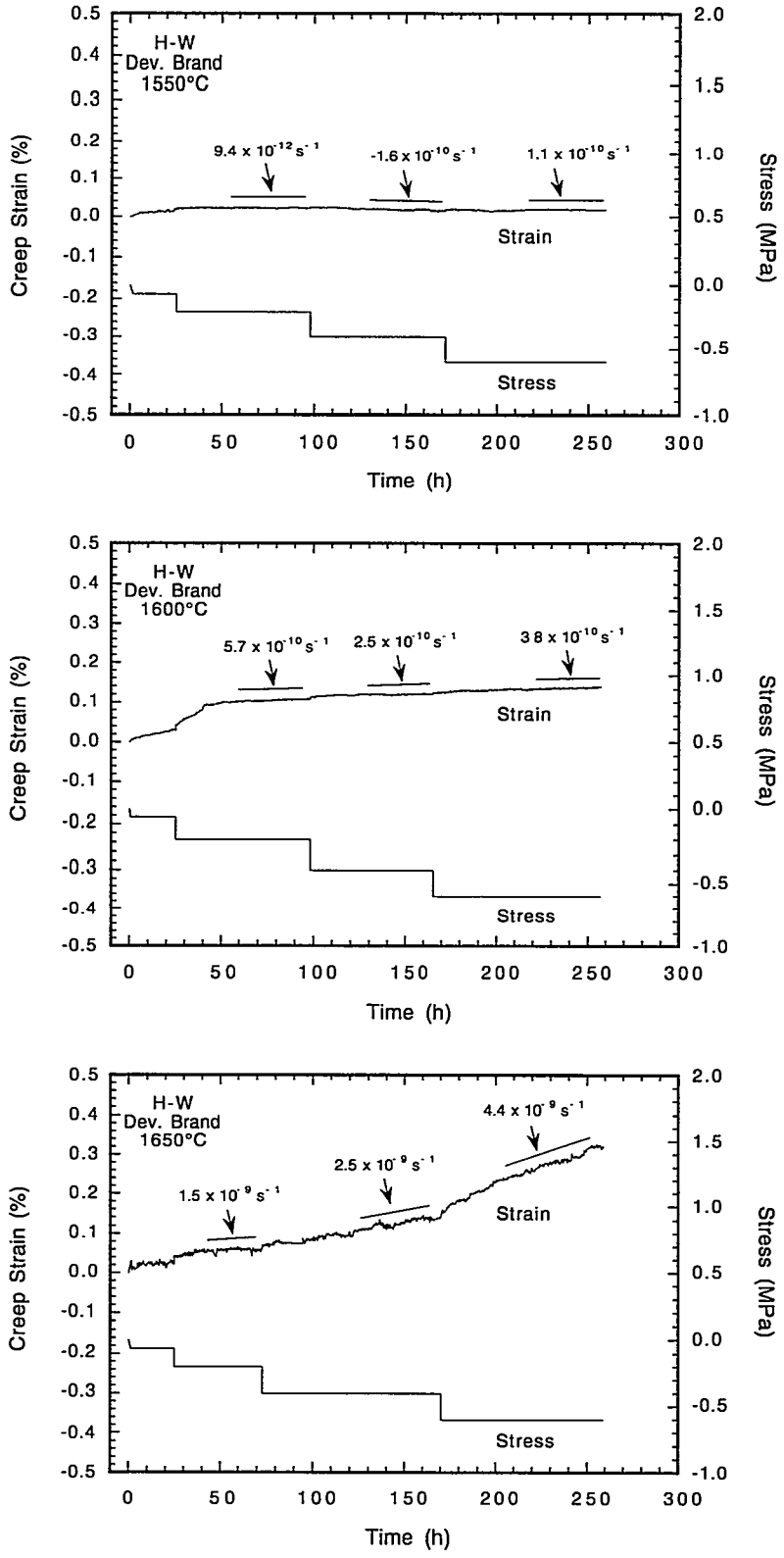

Fig. 20. Creep behavior of H-W's Developmental Brand as a function of temperature.

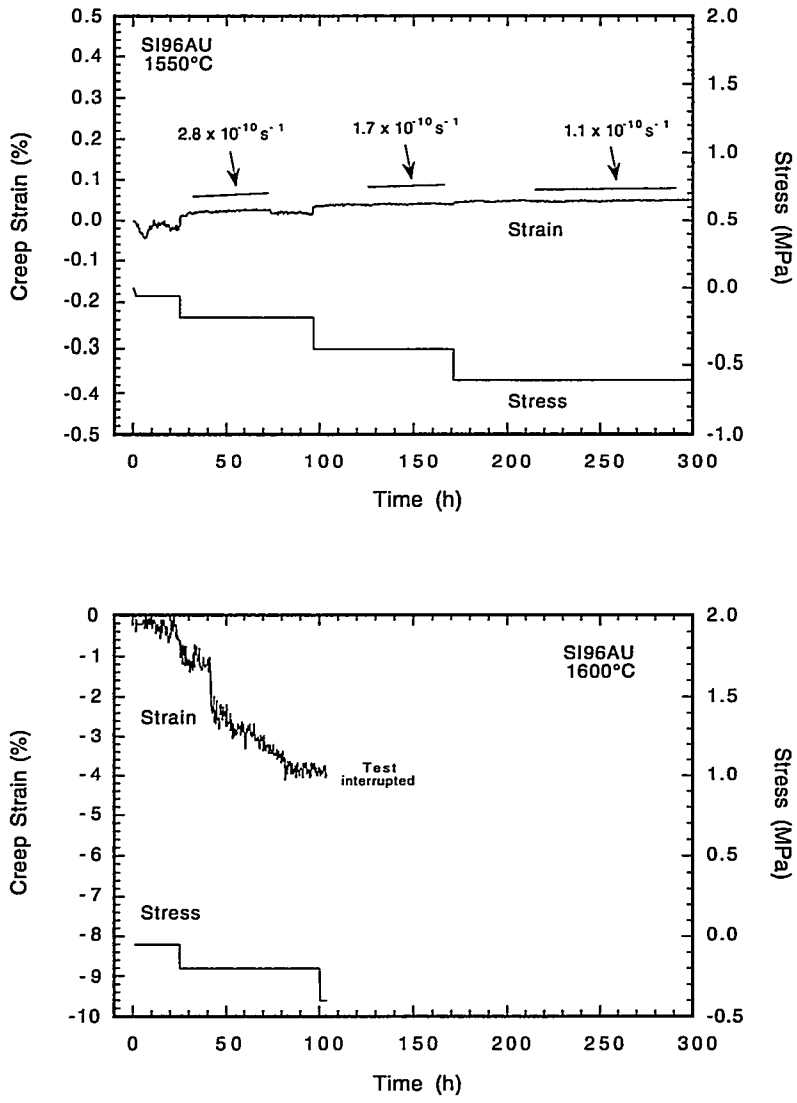

Fig. 21. Creep behavior of SI96AU as a function of temperature.

4.2. CORROSION RESISTANCE

A portion of the silica refractory lid was dissolved by the sodium carbonate vapor forming a liquid phase at temperature. After the test, the maximum amount of recession was measured and summarized in Fig. 22. In general, there was only a slight variation in the amount of attack among the six silicas, and it may be concluded that their corrosion resistances were statistically equivalent.

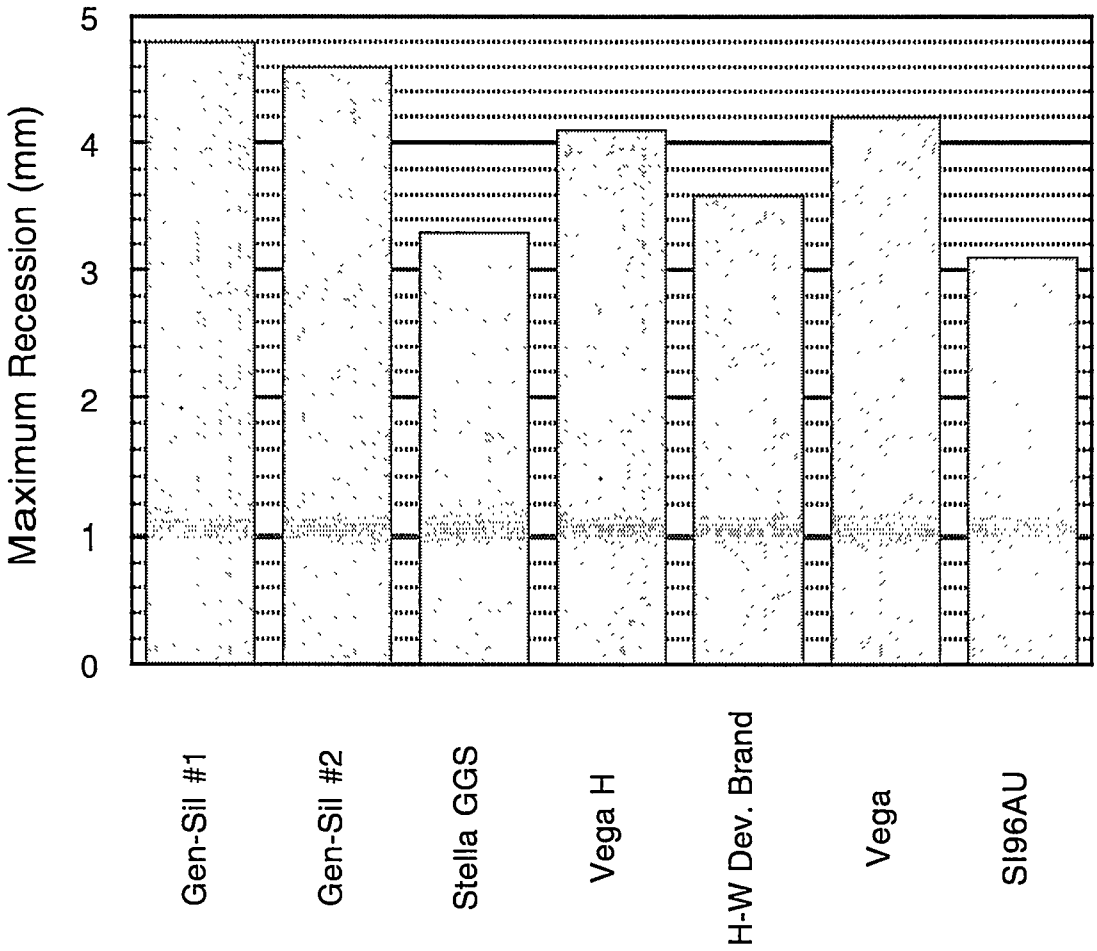

Fig. 22. Amount of refractory recession when exposed to sodium carbonate at 1400°C for 24 hours using ASTM C987 [13].

The amount of recession showed an almost linear relationship with temperature, as shown in Fig. 23. Since a vapor attack is expected, this effect seems reasonable. Varying the amount of sodium carbonate 50% more (18.75 g) and 50% less (6.25 g) from the standard 12.5 g had very little effect. Apparently the sodium carbonate is not fully consumed during the test and the lowest amount does not limit the extent of attack.

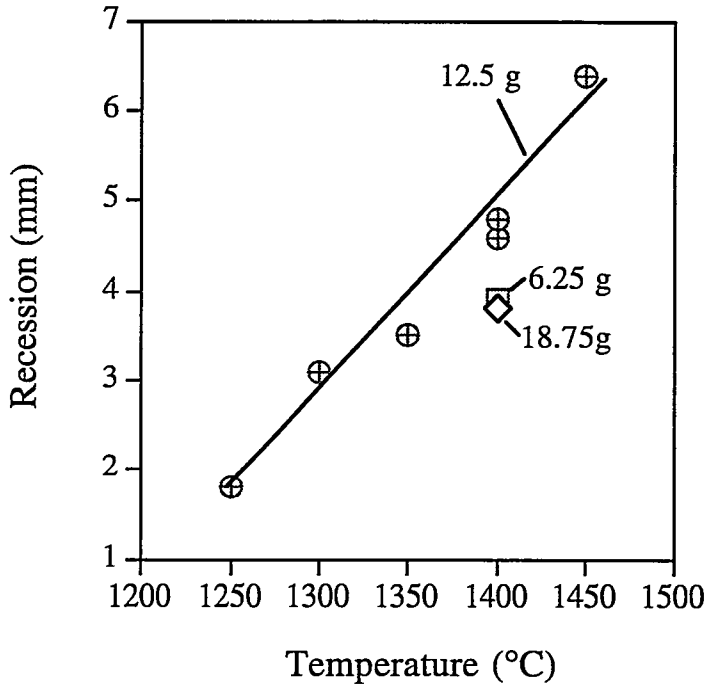

Fig. 23. Amount of recession as a function of temperature and sodium carbonate addition for Gen-Sil silica.

4.3. CHANGES IN BULK CHARACTERISTICS DUE TO CREEP TESTING

4.3.1. Bulk Densities

The measured average bulk densities for the six silica refractories are listed in Table 5. Comparing these values to those reported by the manufacturer (see Table 3) shows that the measured densities are within approximately 2% or less with the exception of SI96AU (measured density 5.7% higher than that reported by the manufacturer).

The change in dimensions of the compressively crept specimens indicated that their size (both diameter and length) had actually *increased* as a consequence of the employed creep test conditions, see Table 6. This expansion phenomenon greatly complicates the creep analysis using Eq. 1 and

likely invalidates its use. All six brands showed this expansion effect. The increases in diameter and length of the creep specimens were between 0.35-1.0%.

Insignificant amounts of secondary phase constituents left the specimens in all refractories when they were tested at 1550°C (cumulative time at temperature approximately 250 hours). A larger fraction of these phases visibly evolved from the specimens at 1600°C (slight glass bubbling on the specimen and fixturing). This phenomenon was quite severe at 1650°C. The density changes in the crept specimens (a net effect of the volume expansion and loss in secondary phase mass) reflect the loss in mass and the volume expansion and ranged from a decrease of 1.6 to 3.9% with a subtle trend of greater density decreases at higher test temperatures (see Table 7). The density decreases among the six brands were statistically equivalent within the data scatter.

Insights into this loss in mass, volume expansion, and density decrease behaviors are described later in the change-in-microstructure discussions based on the RL and CL imaging.

Table 5. Measured bulk densities of "as-received" materials.

	Gen-Sil	SI96AU	Stella GGS	Vega	Vega H	H-W Dev. Brand
Average Bulk Density (g/cc)	1.78	1.85	1.86	1.79	1.87	1.92
Standard Deviation (g/cc)	0.01	0.01	0.02	0.01	0.01	0.01
Number of specimens	11	8	10	10	10	10

Table 6. Dimensional changes of crept specimens. A negative value constitutes contraction and a positive value represents expansion.

	Gen-Sil	SI96AU	Stella GGS	Vega	Vega H	H-W Dev. Brand
1550°C Diameter Change (%)	1.0	0.65	0.45	-0.08	0.49	0.38
1550°C Length Change (%)	0.55	0.55	0.36	0.94	0.42	0.41
1600°C Diameter Change (%)	1.0	9.12	0.42	0.24	0.46	0.38
1600°C Length Change (%)	0.52	-24.0	0.70	0.35	0.47	0.49
1650°C Diameter Change (%)	0.50		0.71	0.50	0.53	0.50
1650°C Length Change (%)			0.47	0.71	0.59	0.46

Table 7. Density changes of crept specimens. A negative value constitutes a decrease in density and a positive value represents an increase.

	Gen-Sil	SI96AU	Stella GGS	Vega	Vega H	H-W Dev. Brand
Density After 1550°C Creep Testing (g/cc)	1.75	1.80	1.81	1.73	1.83	1.90
Density Change (%)	-1.8	-2.6	-1.9	-3.2	-2.8	-1.6
Density After 1600°C Creep Testing (g/cc)	1.73		1.79	1.76	1.82	1.90
Density Change (%)	-2.7		-2.0	-1.8	-1.9	-2.2
Density After 1650°C Creep Testing (g/cc)	1.72		1.79	1.74	1.80	1.88
Density Change (%)	-3.0		-2.2	-3.1	-3.9	-3.0

4.3.2. Crystalline Phases

X-ray diffraction results showed all six as-received silica refractories consisted of cristobalite (PDF# 39-1425) and tridymite (PDF# 18-1170). Even though a calcium silicate was present in the grain boundaries (as detected by SEM/EDS), its concentration was sufficiently small that XRD did not identify it. It was qualitatively determined that Gen-Sil had the highest tridymite content and SI96AU had the highest cristobalite content. The cristobalite to tridymite ratios for the six silicas are shown in Table 8. Very small amounts of quartz were detected only in SI96AU and Vega. Based on the density differences in the silica minerals (quartz - 2.64 g/cc: tridymite - 2.26 g/cc: cristobalite - 2.32 g/cc), it takes the conversion of approximately 6.5% of residual quartz to tridymite or cristobalite to cause a bulk expansion of 1%. Because no quartz was detected in 4 of the conventional silicas, and because its concentration was minute in SI96AU and Vega, this phase change phenomenon could not have caused the volume expansion that these materials exhibited as a consequence of the creep testing.

Table 8. Cristobalite to tridymite ratio in the "as-received" silicas.

Property	Gen-Sil	SI96AU	Stella GGS	Vega	Vega H	H-W Dev. Brand
Cristobalite to Tridymite Ratio	0.75	2.15	2.14	1.42	2.12	2.05

The test conditions that the creep specimens were subjected to changed the phase content in the six silica refractories. The X-ray diffraction spectra of the as-received, 1550°C-tested, and 1650°C-tested silica samples were graphed, compared, and shown in Fig. 24. Being that these two temperatures were the extremes, it was deemed unnecessary to examine the phase content in the creep specimens tested at 1600°C. All the tridymite in these silica refractories was converted to cristobalite during creep tests at 1550°C. The stable silica phase above 1470°C (2680°F) is cristobalite, so these XRD results are not surprising.

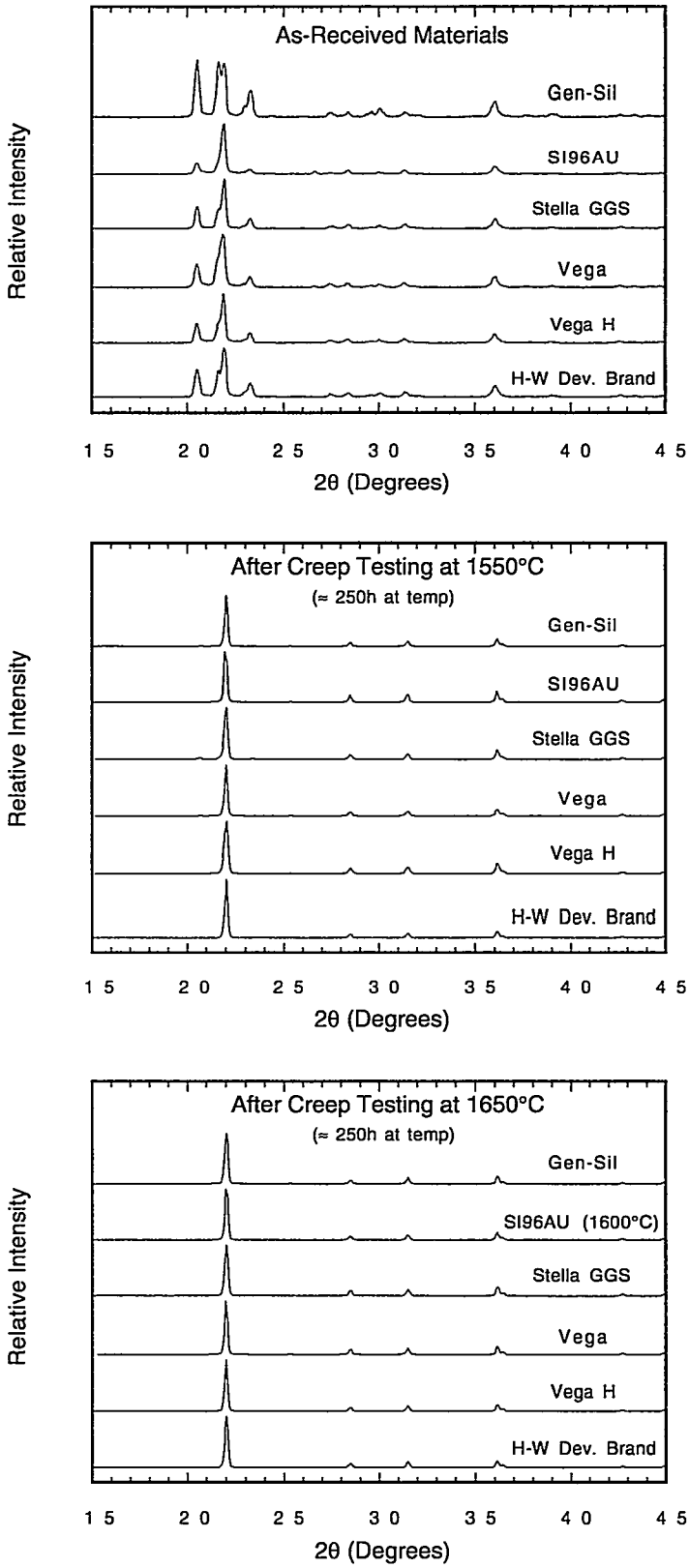

Fig. 24. X-ray diffraction spectra as a function of temperature.

4.3.3. Microstructures

The microstructures of the six silica refractories changed as a consequence of the applied test conditions. The changes of the as-received to the crept microstructures of the six materials had commonality, and these changes are schematically shown in Fig. 25. The as-received silica microstructures of these materials typically consisted of cristobalite aggregates or "islands" in a sea or matrix of prismatic tridymite (approximately 10-20 μm in size near the cristobalite islands, 20-80 μm farther away from them), calcium silicate crystals, and an amorphous silicate. The structure of the cristobalite in these islands often resembled "fish-scales." The individual cristobalite grains comprising the cristobalite islands have a rather uniform size distribution, 5 to 10 μm across, while the size of the cristobalite islands ranged from approximately 40 μm to more than 1 mm. The primary difference among the relative amounts of cristobalite and tridymite among the materials was described in Section 4.3.2. During creep testing at 1550, 1600, and 1650°C, the tridymite converted to cristobalite, and a new amorphous silicate (located between the new and growing cristobalite islands) formed. Additionally, many of the crept cristobalite microstructures contained pores that resembled "tunnels"; they appeared to be avenues for vaporization, but their structure was not examined so their cause is not known.

Both RL and CL imaging supplemented one another well to explore these microstructural changes. The RL images of the as-received and crept microstructures are shown for Gen-Sil, SI96AU, Stella GGS, Vega, Vega H, and Harbison-Walker's developmental brand respectively in Figs. 26-31. Pores, tridymite, and Ca-silicate (described in greater detail in Section 4.3.4) are labeled and were consistently observed in the as-received microstructures of each refractory. The creep testing temperatures changed this microstructure to those shown in Figs. 26-31; these changes included the formation of larger pores, larger cristobalite islands, the new amorphous silicate, and the creation of gaseous pores. The bulk expansion of the crept specimens may be explained by the destruction of original tridymite bonds and the enlargement of pores and of the cristobalite islands.

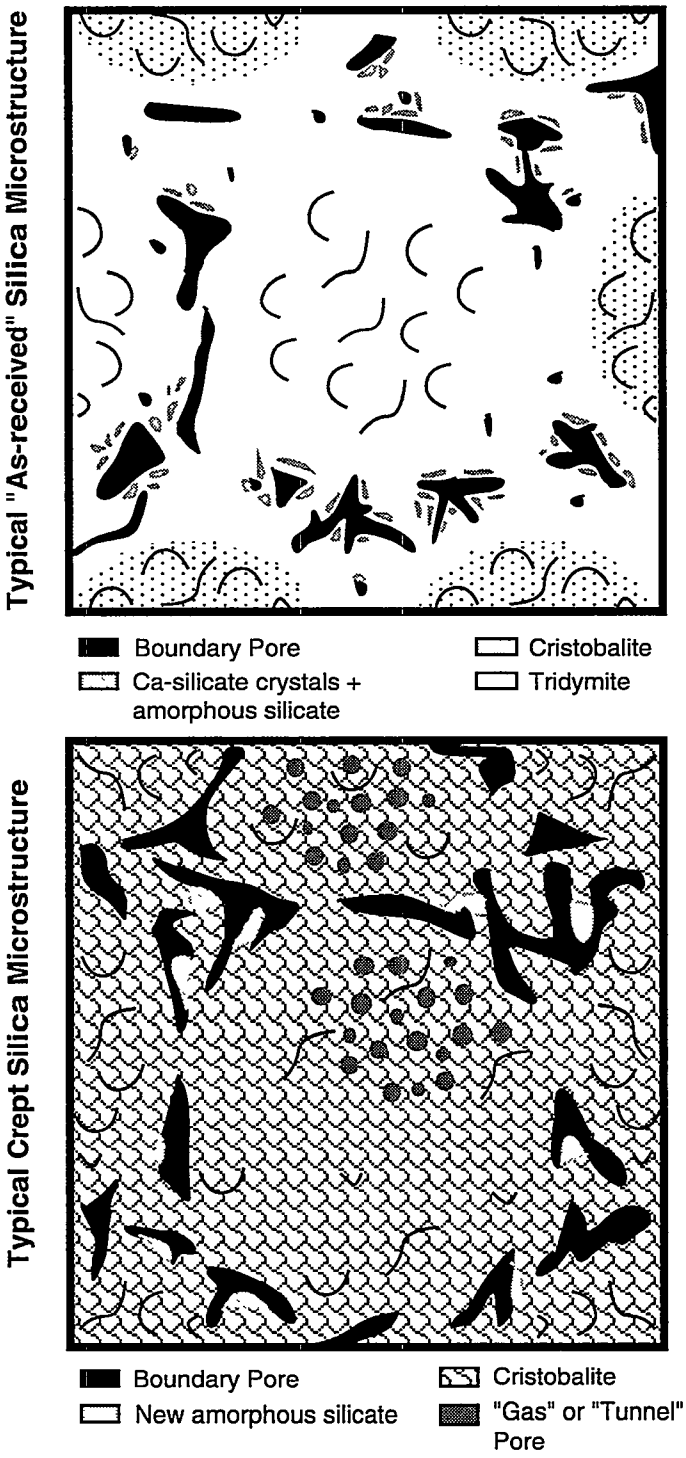

Fig. 25. Schematic of the change in microstructure from the "As-Received" material state to that after creep or high temperature exposure.

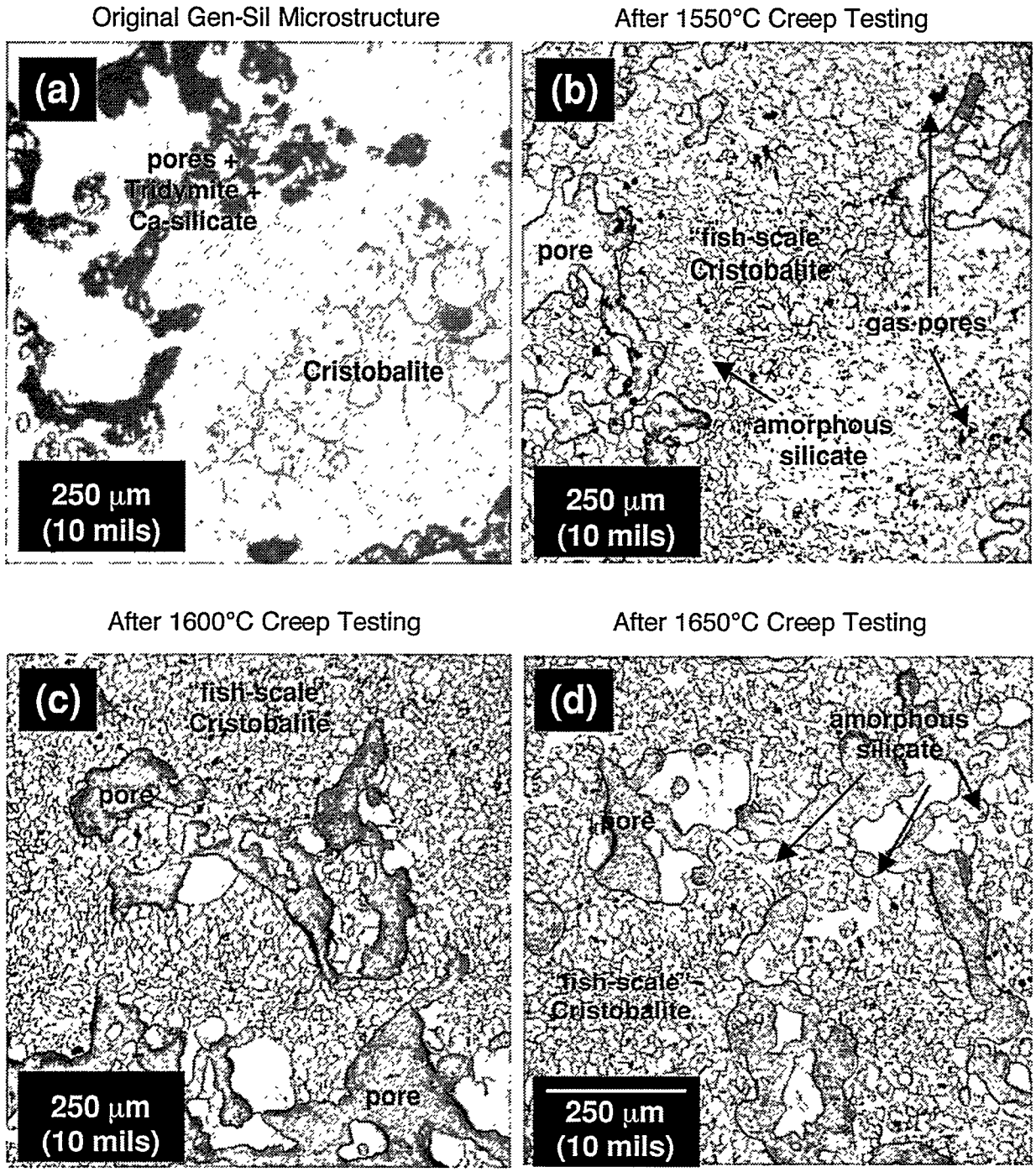

Fig. 26. Gen-Sil's microstructural changes as a function of temperature as revealed by reflected light microscopy.

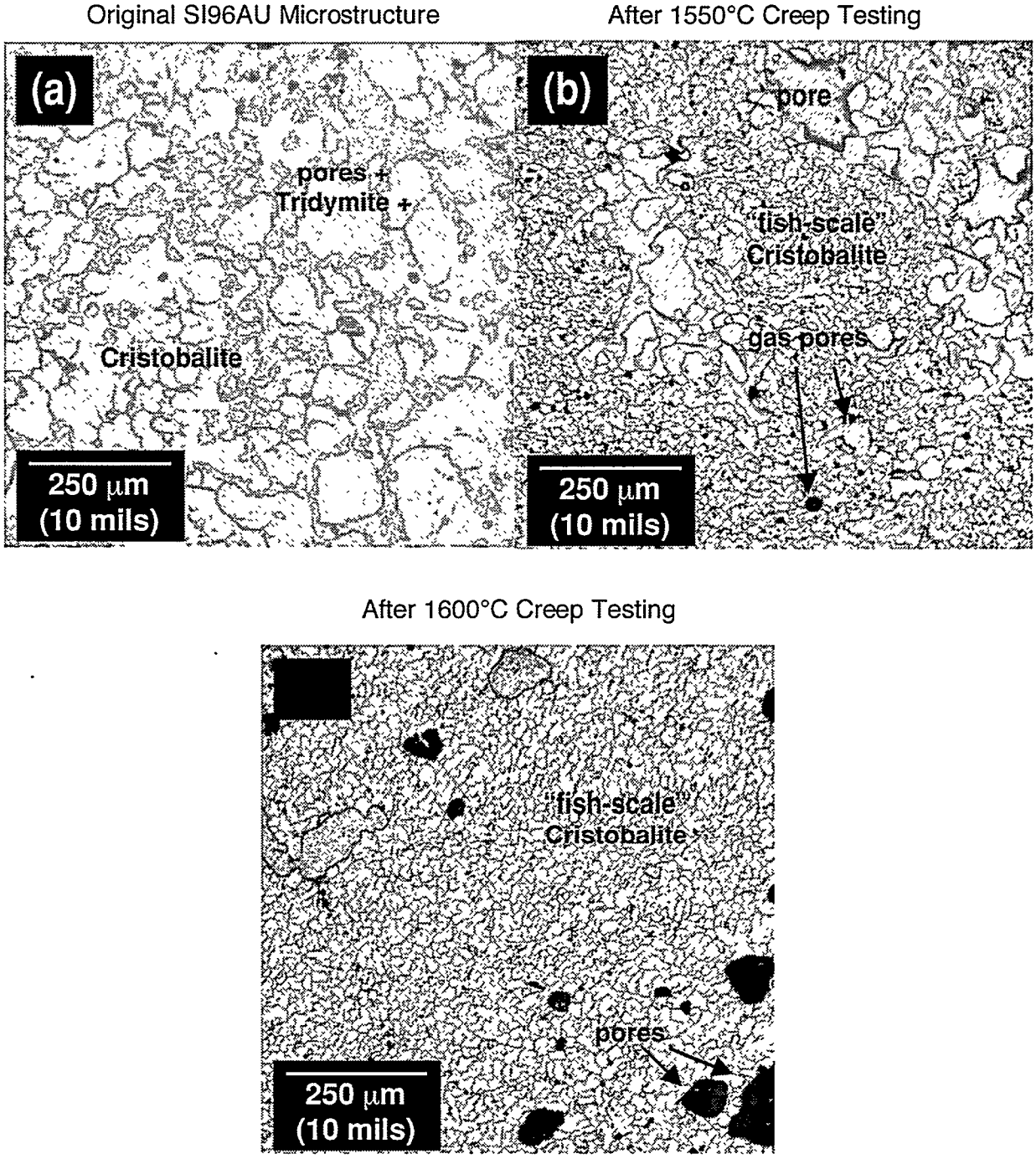

Fig. 27. SI96AU's microstructural changes as a function of temperature as revealed by reflected light microscopy.

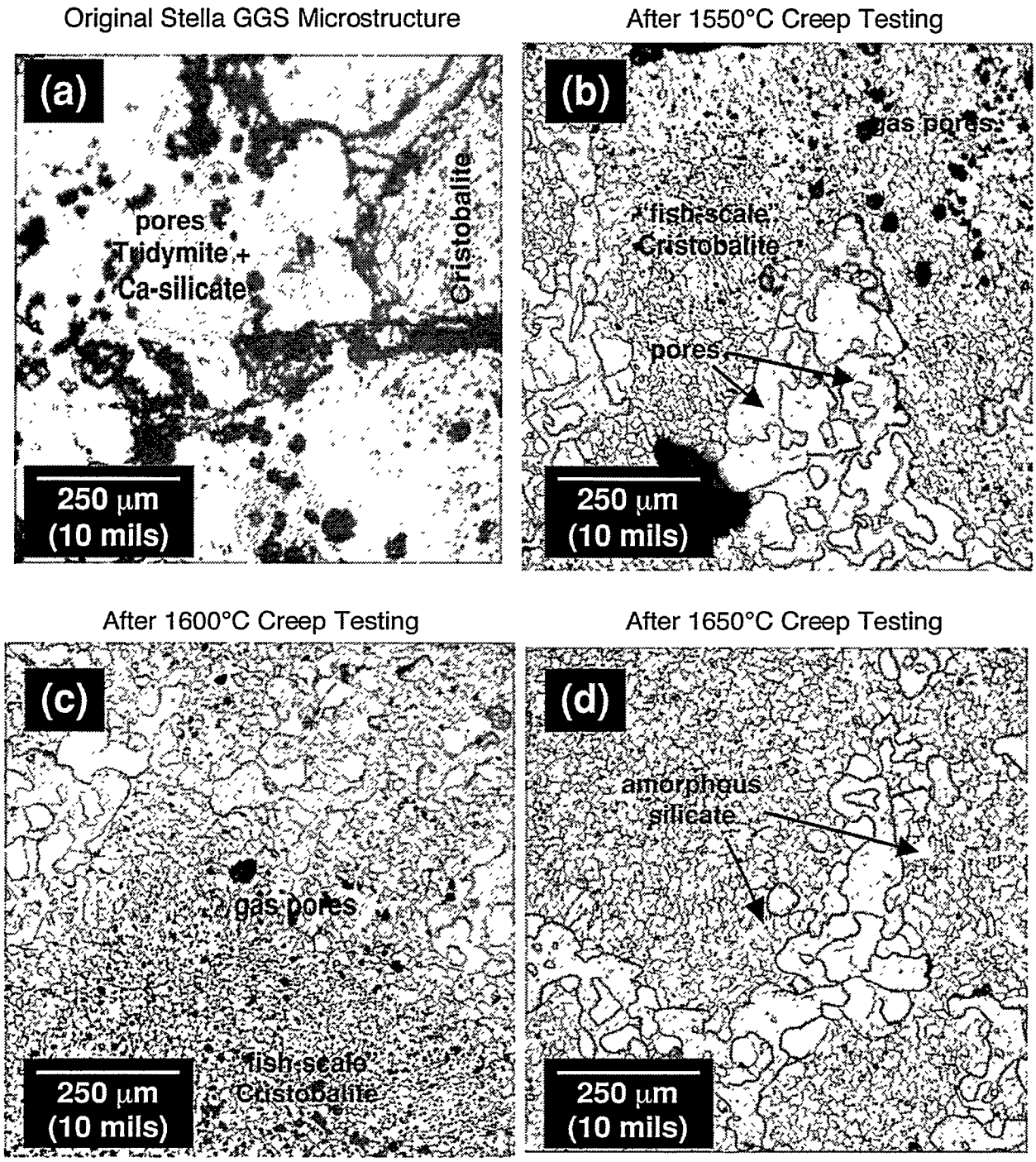

Fig. 28. Stella GGS's microstructural changes as a function of temperature as revealed by reflected light microscopy.

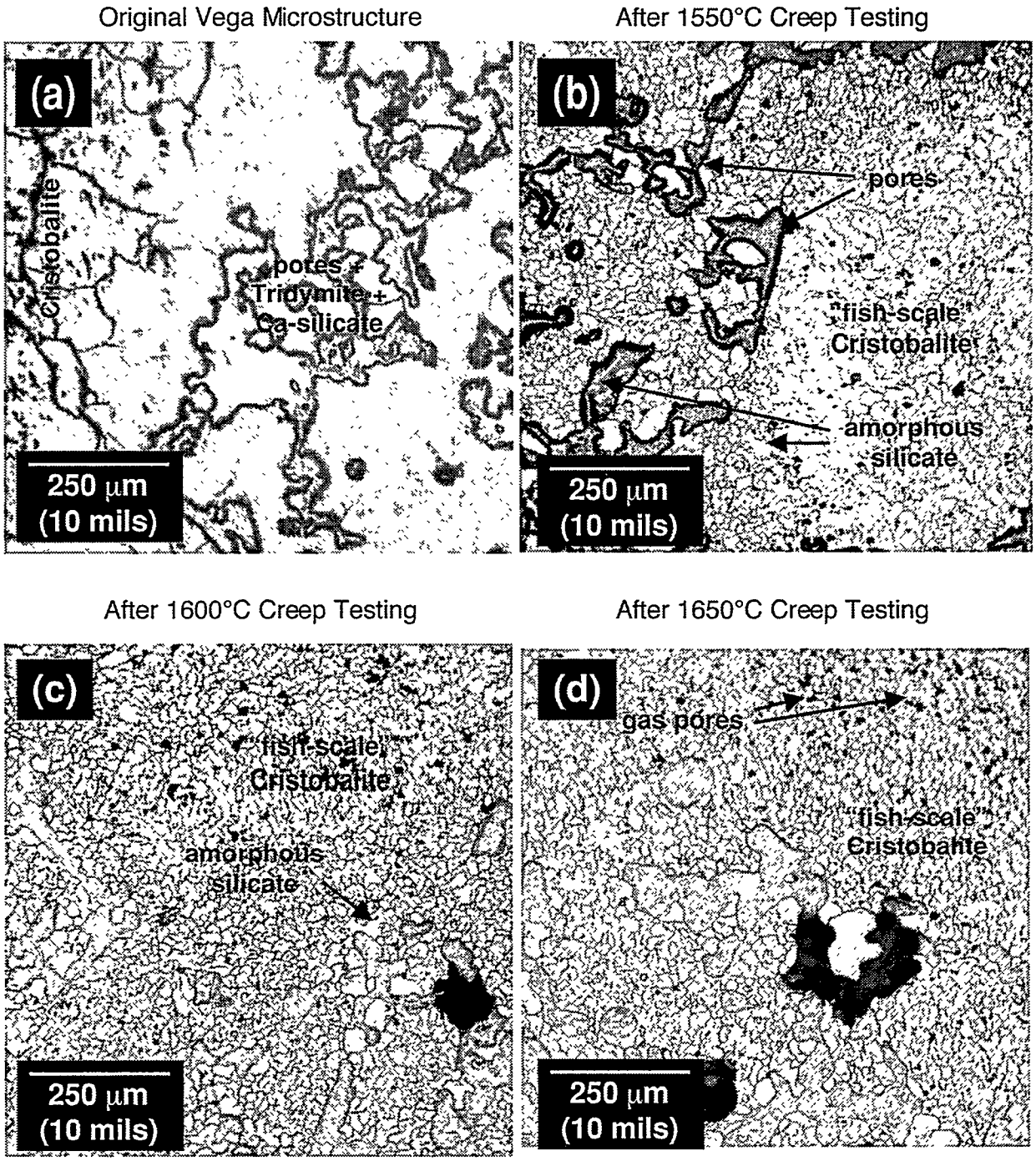

Fig. 29. Vega's microstructural changes as a function of temperature as revealed by reflected light microscopy.

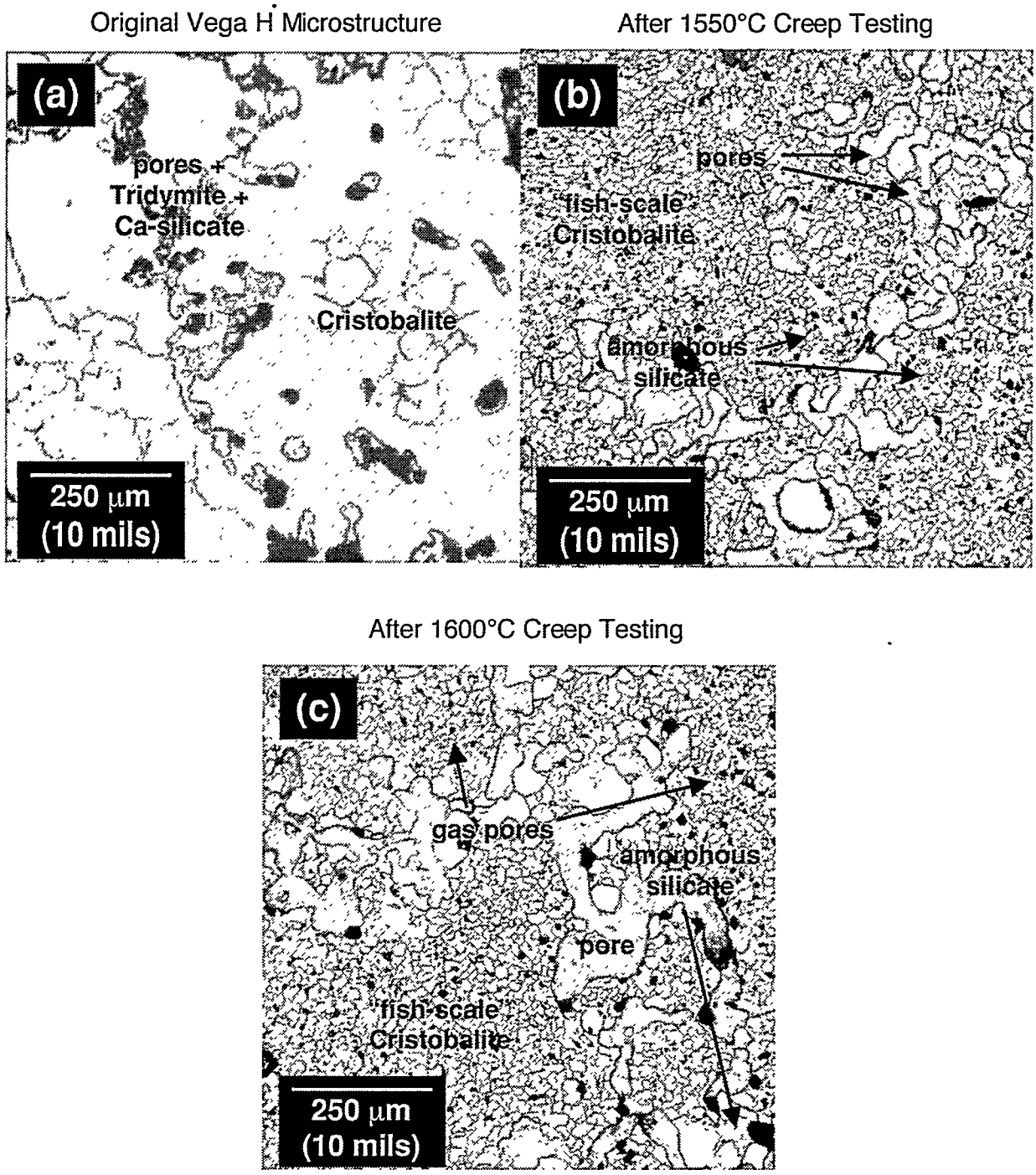

Fig. 30. Vega H's microstructural changes as a function of temperature as revealed by reflected light microscopy.

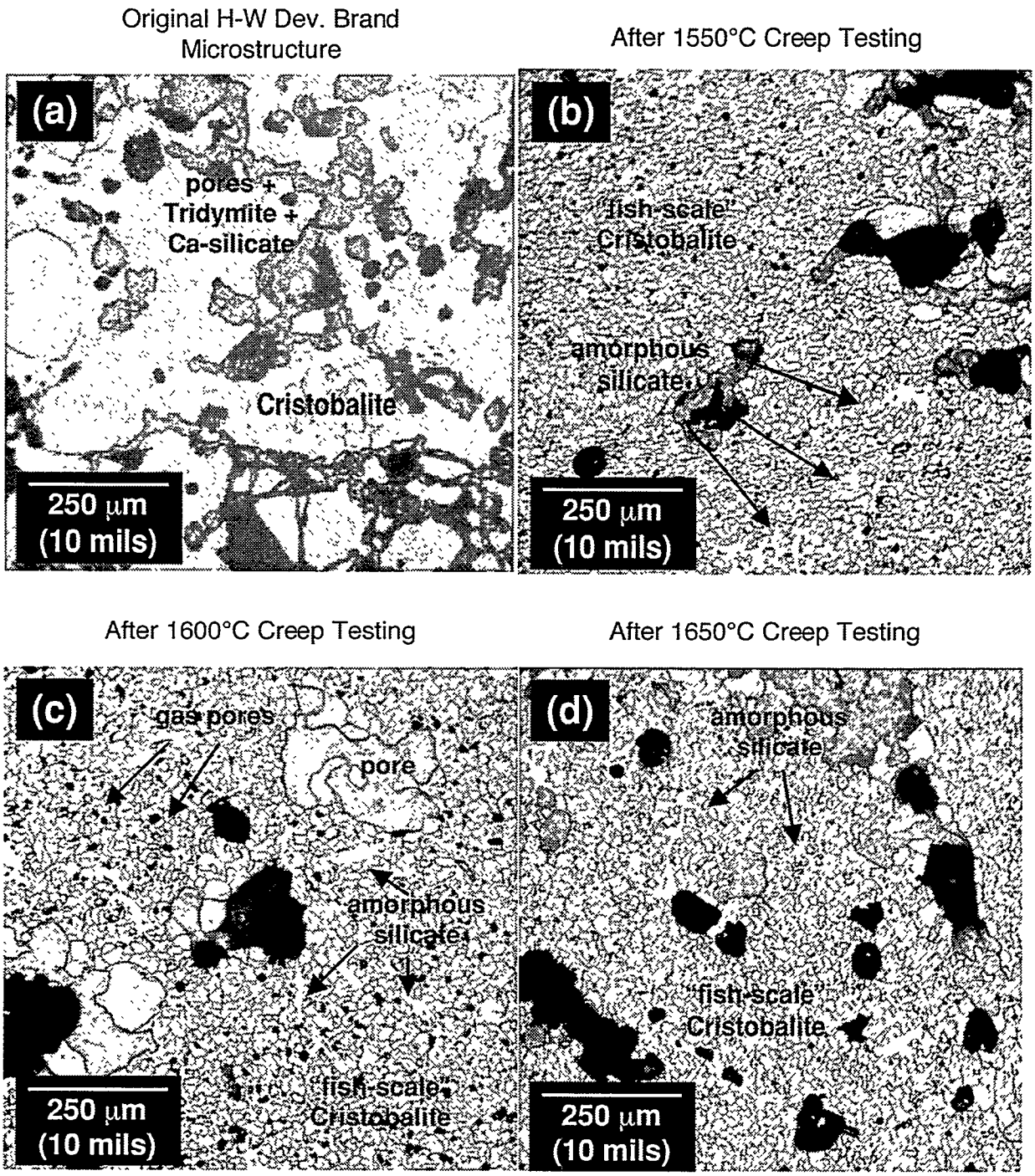

Fig. 31. Harbison-Walker's developmental brand's microstructural changes as a function of temperature as revealed by reflected light microscopy.

Cathodoluminescence imaging provided an interesting and different perspective into how the microstructures changed as a consequence of the creep testing. The CL imaging revealed the tridymite in the as-received state better than the RL imaging, and it also provided new insights into how the cristobalite islands changed or grew. The CL images of the as-received and crept microstructures are shown for Gen-Sil, SI96AU, Stella GGS, Vega, Vega H, and Harbison-Walker's developmental brand respectively in Figs. 32-37. The as-received cristobalite islands luminesced dark blue while the tridymite luminesced a lighter blue.

The cristobalite islands imaged by CL showed an interesting pattern in the crept specimens. The cores of most of the cristobalite aggregates in these specimens exhibited a light blue color while their outer zones or rims were dark blue. The light blue core represents the original fish-scale cristobalite island. The core or center of these islands after creep testing is relatively free of impurity phases resulting in the light blue CL color. During the creep testing, the tridymite converted to cristobalite or added to the size of existing cristobalite islands. Additionally, the original calcium and amorphous silicates (containing transition metals and alkalis to be described in Section 4.3.4) formed a liquid phase during creep testing that either diffused into the enlarging cristobalite islands or was present during their growth: this outer zone or rim was characterized by dark blue CL in Figs. 32-37.

The Ca-silicate phase luminesced bluish-white and locally bright yellow, with some of its crystals being as small as 15 μm, in the as-received microstructures. However, during creep testing, iron impurities in the original amorphous silicate combined with the Ca-silicate phase to form a new amorphous silicate that did not produce CL color due to the presence of the iron.

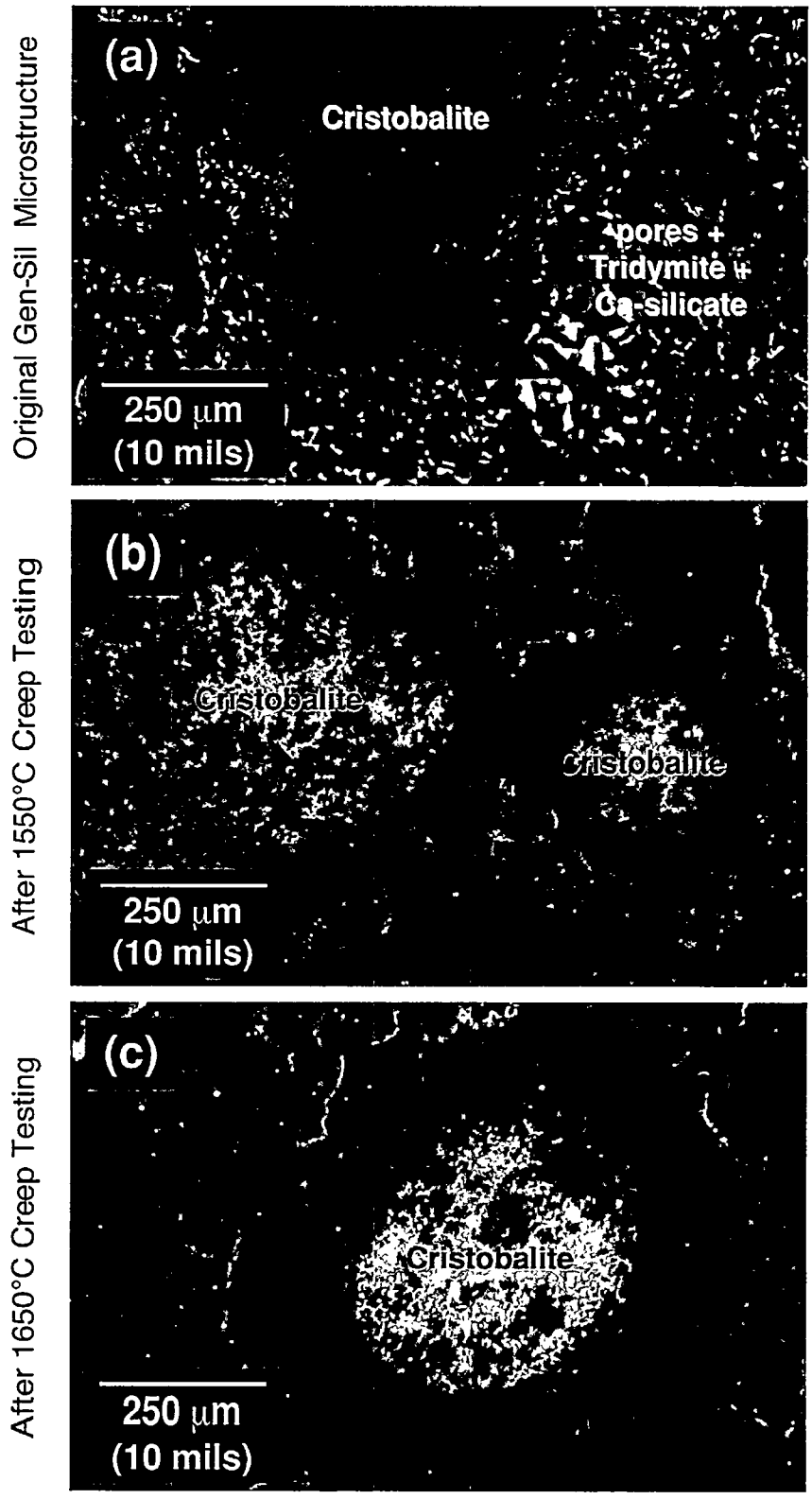

Fig. 32. Gen-Sil's microstructural changes as a function of temperature as revealed by cathodoluminescence imaging.

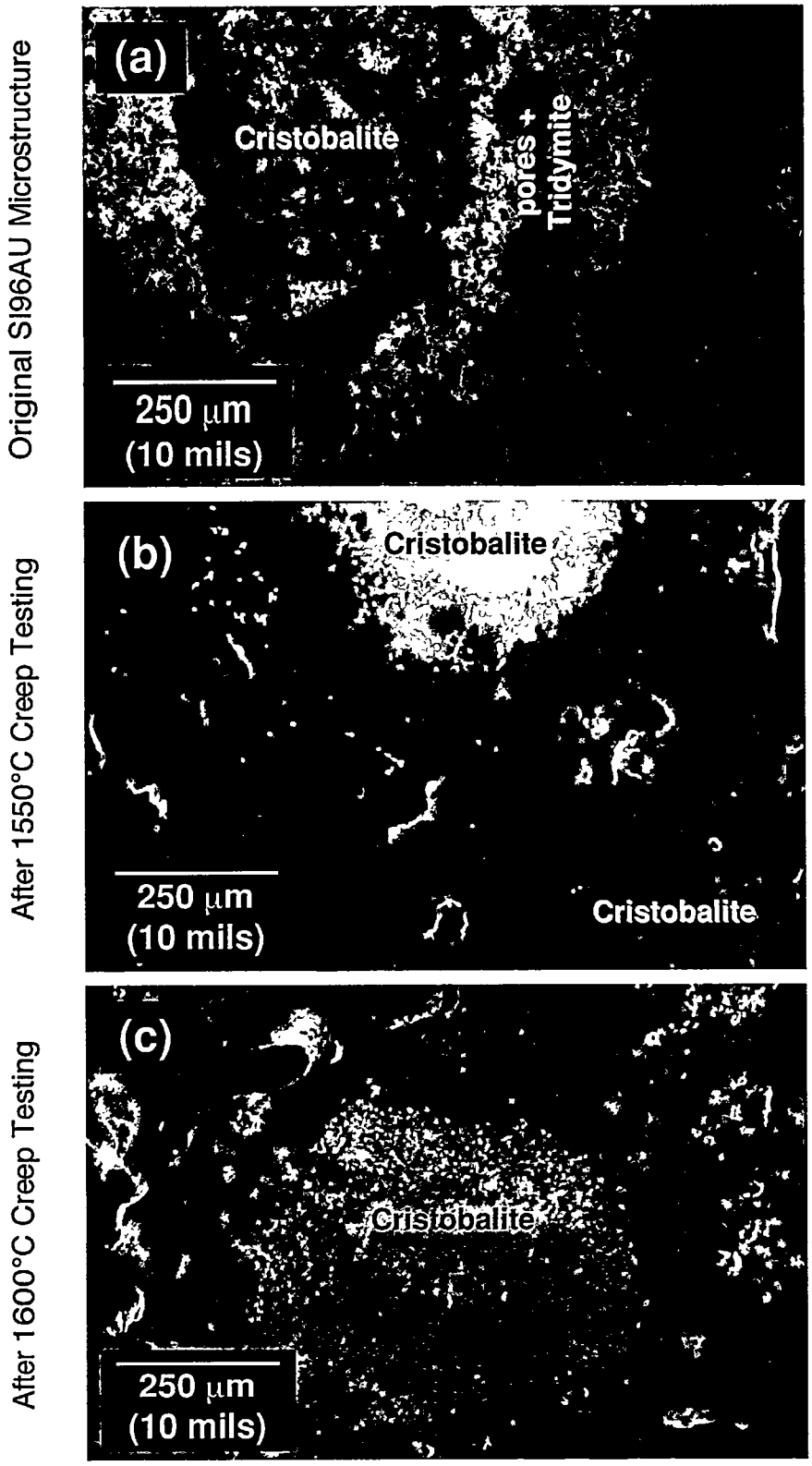

Fig. 33. SI96AU's microstructural changes as a function of temperature as revealed by cathodoluminescence imaging.

Original Stella GGS Microstructure

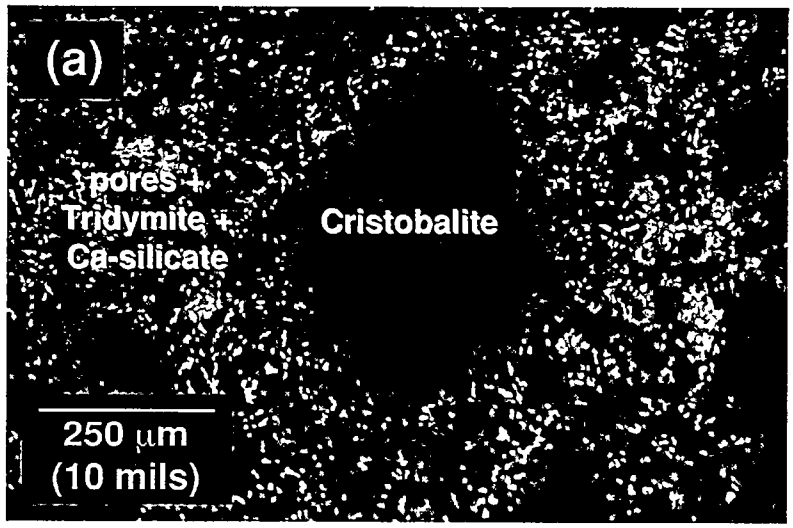

After 1600°C Creep Testing

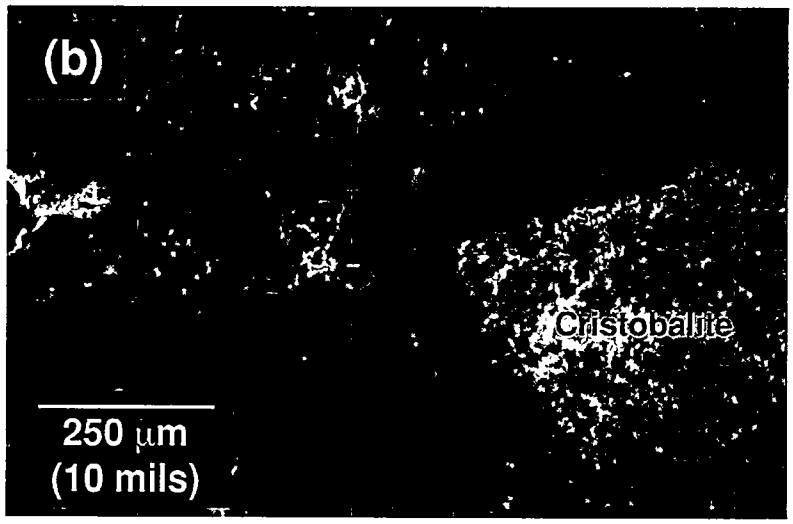

Fig. 34. Stella GGS's microstructural changes as a function of temperature as revealed by cathodoluminescence imaging.

Original Vega Microstructure

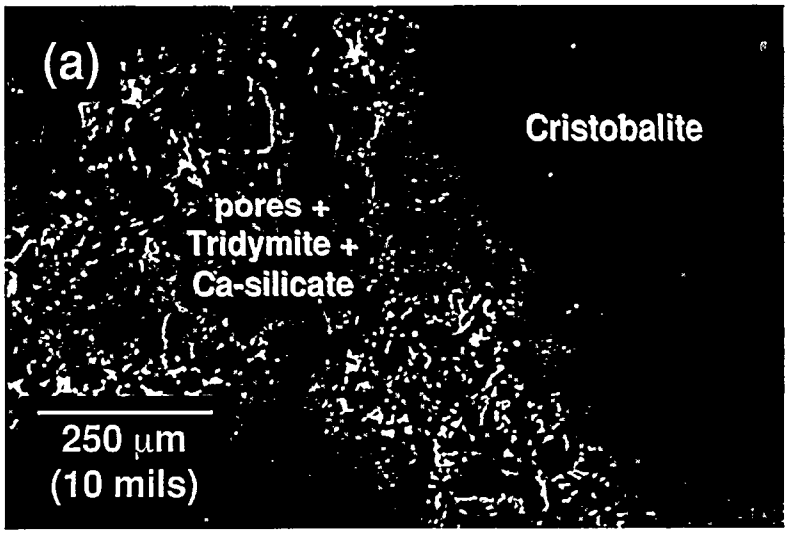

After 1600°C Creep Testing

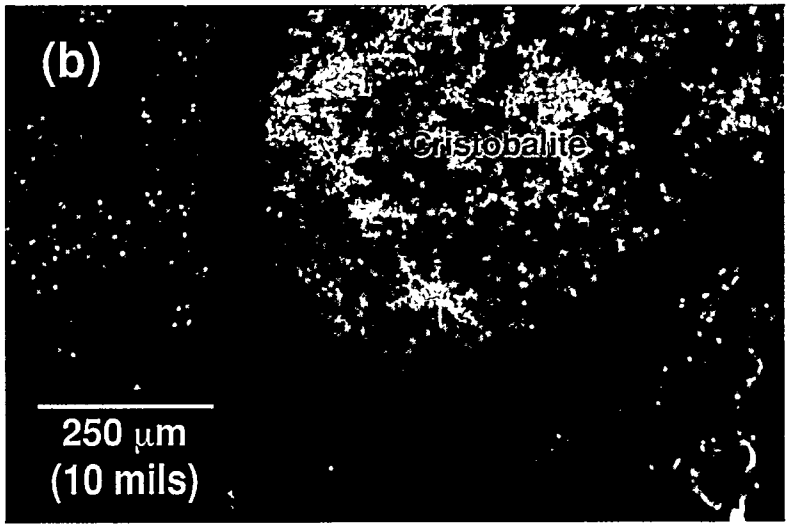

Fig. 35. Vega's microstructural changes as a function of temperature as revealed by cathodoluminescence imaging.

Original Vega H Microstructure

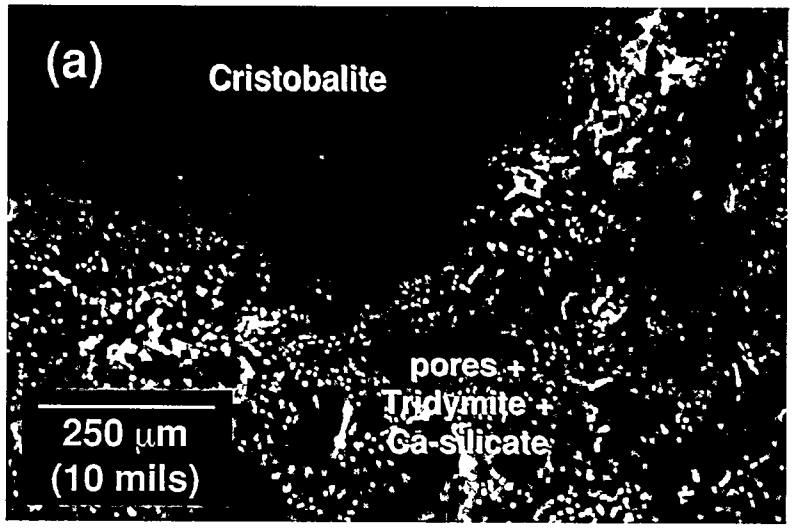

After 1550°C Creep Testing

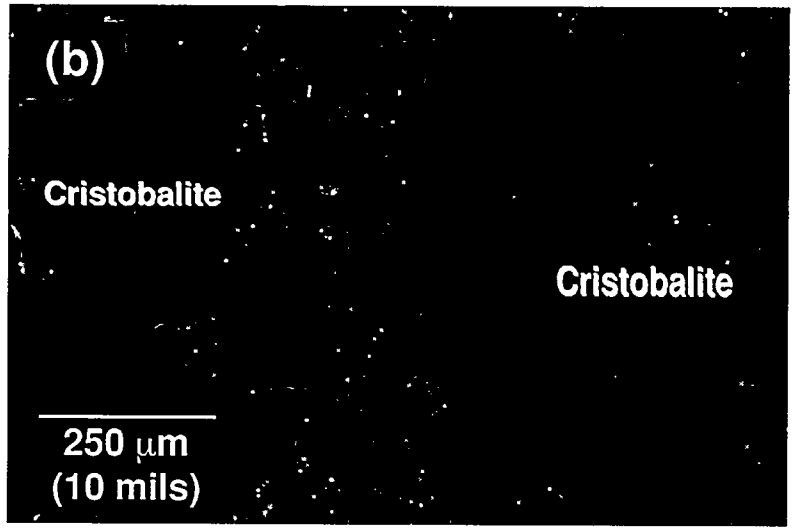

Fig. 36. Vega H's microstructural changes as a function of temperature as revealed by cathodoluminescence imaging.

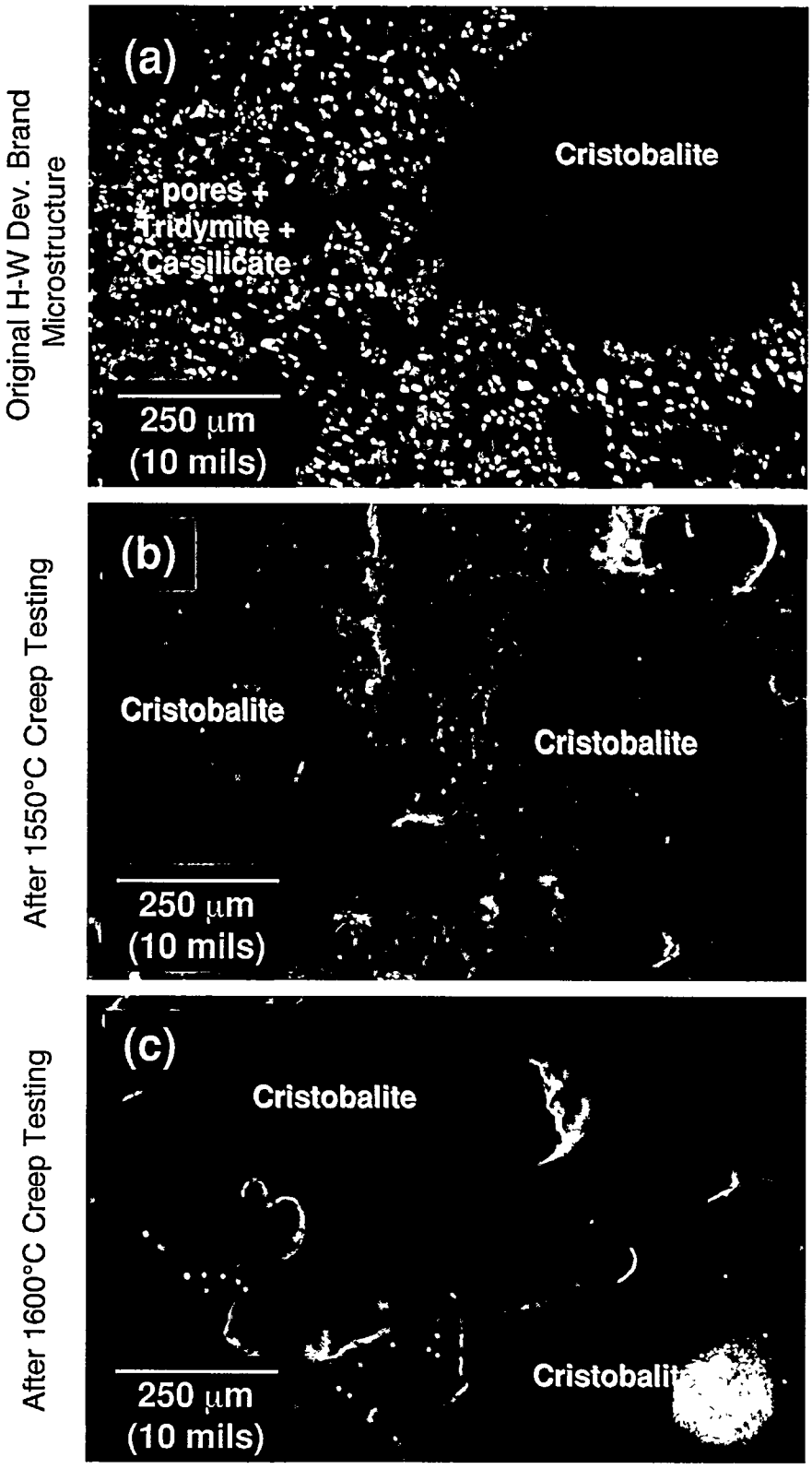

Fig. 37. Harbison-Walker's developmental brand's microstructural changes as a function of temperature as revealed by cathodoluminescence imaging.

4.3.4. SEM/EDS

The compositions of the secondary phase glass in the original and 1600°C crept refractories were examined using SEM/EDS. The original secondary phase in all the silicas, with the exception of SI96AU, was actually comprised of two distinct phases. One phase in these five silicas was a pure Ca-silicate phase with a chemistry of approximately 62% CaO and 38% SiO_2, which is indicative of the presence of $2CaO \cdot SiO_2$. EDS analysis showed that the other secondary phase in the as-received state of these five silicas contained FeO, K_2O, Al_2O_3, MgO, or TiO_2. The presence of these impurities is important for the fluxing of cristobalite and for the formation of tridymite. The secondary phase in SI96AU was exceptionally glassy and did not consist of two separate phases. SI96AU's composition was characterized by the presence of a relatively high TiO_2 and Al_2O_3 content (the latter consistent with its "Type B" silica classification).

The examination of the composition of the secondary phase in the crept specimens provided results which permitted a qualitative comparison with the manufacturer's stated content in these six silica refractories. For the most part, the secondary constituents that the manufacturers claimed were in their supplied materials were correct. The trend and relative amounts of Fe_2O_3 listed in Table 2 closely matched those measured by EDS and listed in Table 9. SI96AU was reported to have the highest CaO content of the six refractories by its manufacturer; however, the present EDS analysis indicated that it had the least. MgO amounts were indeed small, as reported by the manufacturer, with the three examined Harbison-Walker refractories containing the least. SI96AU was reported to contain appreciably more TiO_2 and EDS supported that claim. The alkali (potassium) content measured by EDS showed that SI96AU had the most and the three Harbison-Walker silicas had the least; the former result was consistent with the manufacturer's reported data but not the latter.

Table 9. Chemical analysis of grain boundary phase in specimens crept at 1600°C. The values shown are averages of a minimum of two different EDS analyses.

Constituent	Gen-Sil (at. %)	SI96AU (at. %)	Stella GGS (at. %)	Vega (at. %)	Vega H (at. %)	H-W Dev. Brand (at. %)
Si	15.54	16.77	17.23	15.78	15.99	17.21
Ca	17.55	13.60	18.98	20.07	18.31	16.01
Fe	5.74	2.33	1.64	4.06	4.27	4.02
Al	0.99	3.12	1.44	0.76	1.44	2.12
Ti	0.03	1.88	-	-	0.04	-
K	0.40	1.08	0.61	-	0.29	0.33
Mg	0.41	0.80	0.87	0.23	0.39	0.27
O	59.34	60.42	59.23	59.10	59.27	60.04

4.4. EFFECT OF TEMPERATURE

Consistent with bulk changes exhibited by the creep specimens, the unstressed or "aged" silica refractory specimens from all six materials also exhibited loss of mass, dimensional increases, and density decreases between 1550-1650°C.

The mass losses of the six brands at 1550 and 1600°C were equivalent; however, some silica brands lost more mass than others at 1650°C: Harbison-Walker's developmental brand lost approximately 0.1% of its mass; SI96AU lost ≈ 0.2%; Vega H lost ≈ 0.3%; Gen-Sil lost ≈ 0.5%; Vega lost ≈ 1.0%; and Stella GGS lost ≈ 1.5%. The majority of the mass loss occurred in less than 25 hours for all six brands. These trends are illustrated in Fig. 38.

The dimensional increases of the silica specimens were a function of temperature as illustrated in Fig 39. Additionally, some brands expanded more than others. Each of the specimens expanded isotropically in each of three directions (within statistical confidence). The ranges of expansion were ≈ 1-2.5% at 1550°C, ≈ 2.25-3.75% at 1600°C, and ≈ 3.5-6% at 1650°C. Harbison-Walker's developmental brand expanded the least amount at all three temperatures followed by Gen-Sil. The ascending order of expansion for the other four brands varied with temperature. Stella GGS expanded the most at 1550°C (≈ 2.5%), SI96AU expanded the most at 1600°C (≈ 3.75%), and Vega expanded the most at 1650°C (≈ 6%). Dimensional increases in these aged specimens were greater than axial expansion of the crept silica specimens at the same temperatures indicating that there may have been a specimen-size-effect. As discussed in Section 4.3.3, the change in the as-received assemblage of tridymite, amorphous silicate, Ca-silicate, and cristobalite to the crept microstructure consisting entirely of cristobalite likely caused the observed volume expansion: the

same phenomenon appeared to have occurred in these aged specimens. Temperature is the activator of this phenomenon and the application of stress is not a prerequisite for it.

The density decreases of the silica specimens were a function of temperature as shown in Fig. 40. Additionally, some brands became less dense than others. The changes in density are a consequence of the above described changes in mass and volume. The ranges of density decreases were ≈ 1-2.75% at 1550°C, ≈ 2.25-4.0% at 1600°C, and ≈ 3.5-7.0% at 1650°C. The density of Harbison-Walker's developmental brand changed the least of the six brands at all three temperatures. The ascending order of density for the other five brands varied with temperature. The density of Stella GGS decreased the most at 1550°C (≈ 2.75%), that for SI96AU decreased the most at 1600°C (≈ 4%), and that for Vega decreased the most at 1650°C (≈ 7%).

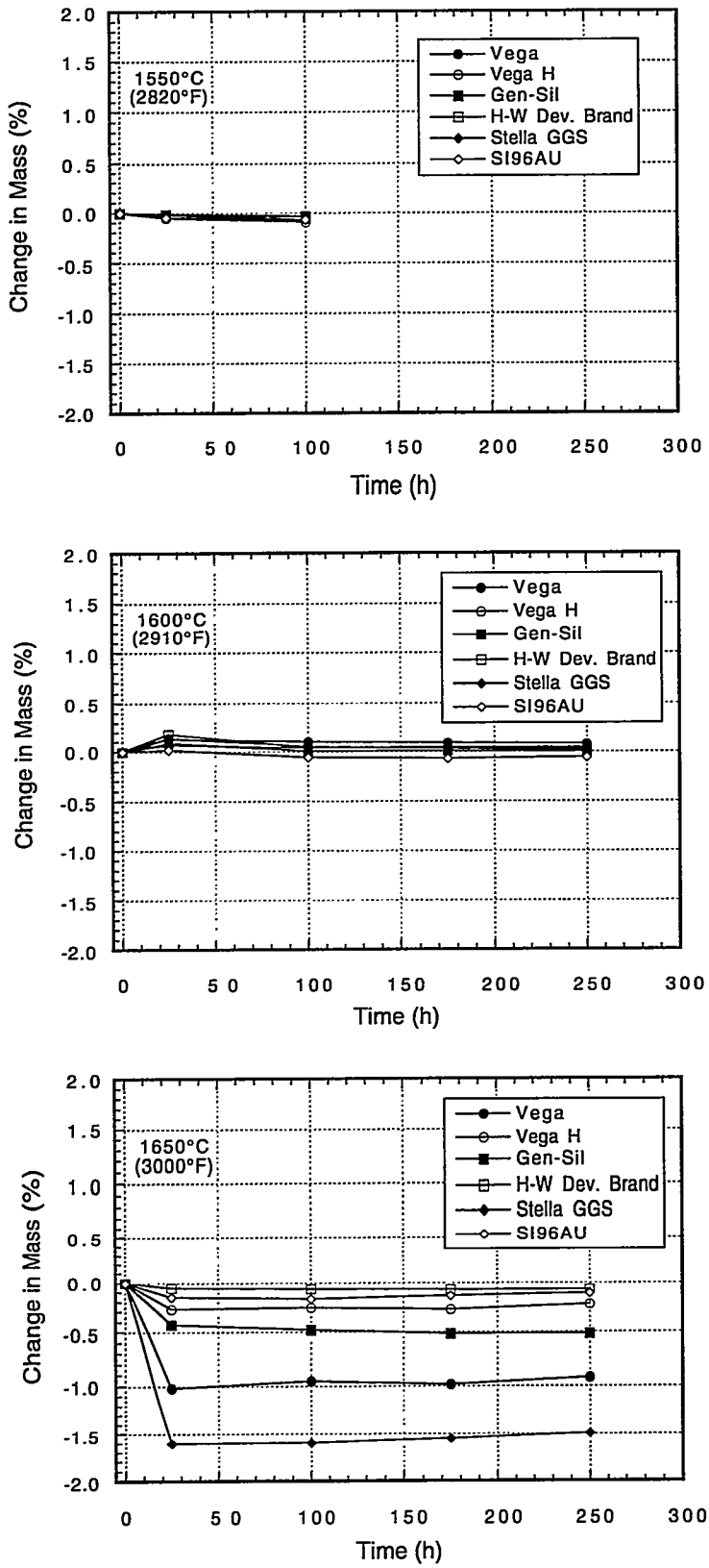

Fig. 38. Change in mass of "aged" specimens as a function of time and temperature.

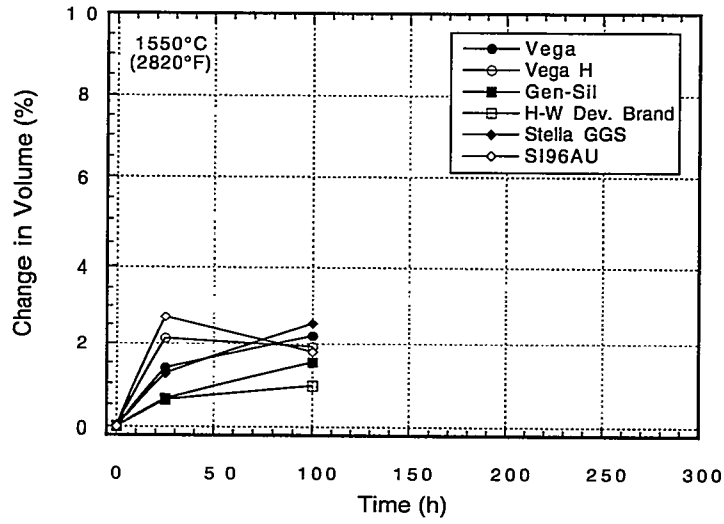

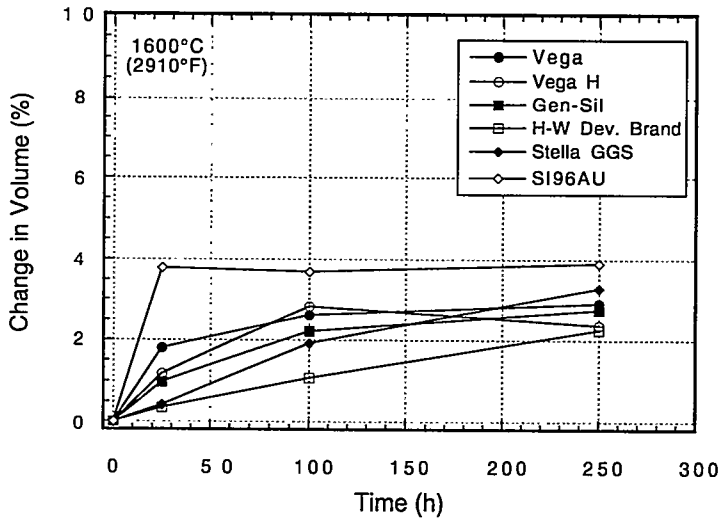

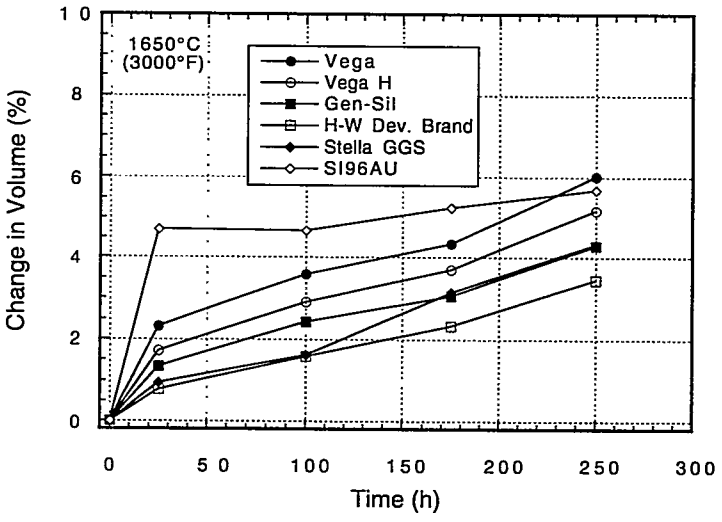

Fig. 39. Change in volume of "aged" specimens as a function of time and temperature.

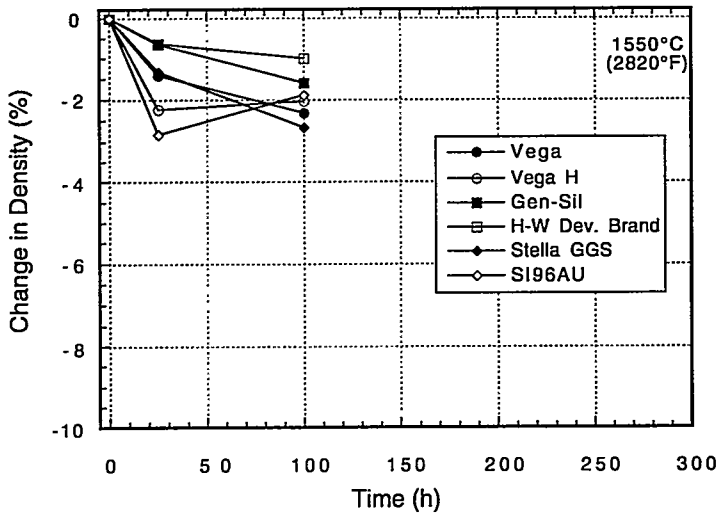

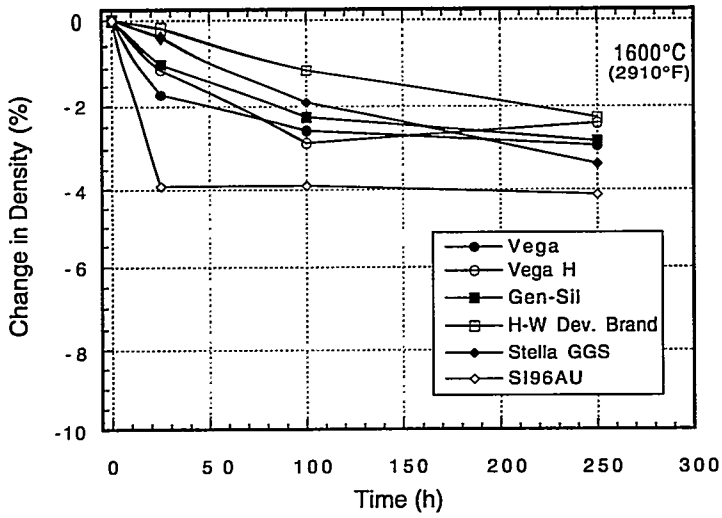

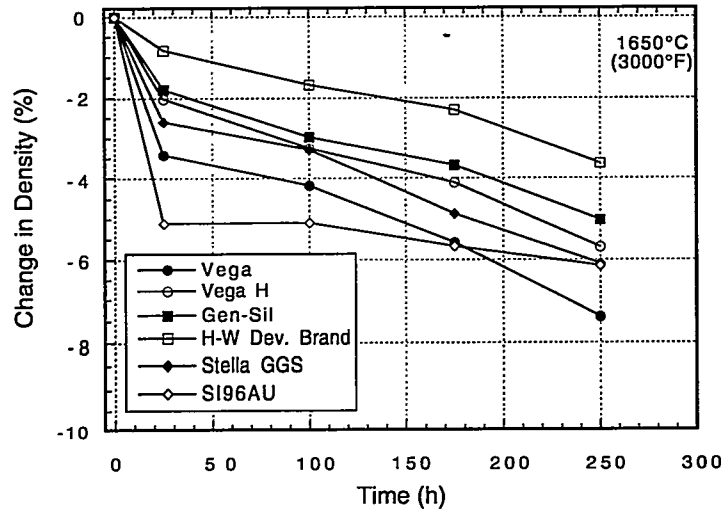

Fig. 40. Change in density of "aged" specimens as a function of time and temperature.

5. CONCLUSIONS

- The amount of compressive creep of Gen-Sil, Stella GGS, Vega, Vega H, and Harbison-Walker's new developmental brand (flux factors less than 0.5% or "Type A" for all five of these brands) conventional silica was negligible at temperatures between 1550-1650°C (2820-3000°F) and at compressive stresses between 0.2 to 0.6 MPa (29-57 psi). Only one specimen per condition was tested so the authors were unable to statistically conclude that any one of these five brands had superior creep resistance to the others; however, if differences do indeed exist, then they are believed to be insignificant.
- The compressive creep of SI96AU (flux factor greater than 0.5% or "Type B") conventional silica was negligible at 1550°C. However, SI96AU deformed (contracted) by more than 20% at 1600°C at stresses between 0.2-0.6 MPa. This behavior was inferior to that of the other five tested brands. SI96AU was not creep tested at 1650°C; however, its creep deformation was expected to still be inferior to the other five silica brands.
- The compressive creep rates of all six brands were not able to be represented as a function of temperature and compressive stress using the conventionally used Arrhenius Norton-Bailey creep equation (*i.e.*, the Arrhenius power-law creep model). Concurrently active mechanism(s), other than creep, resulted in larger or oppositely anticipated dimensional changes than those produced by creep; this effect limited the ability to identify or interpret the lesser-active creep mechanism in these silica refractories. Models other than Norton-Bailey (or equivalent "creep" models that represent creep rate as a function of temperature and stress) should be used to represent or predict the long-term dimensional stability of conventional silica superstructures that are subjected to compressive stresses less than 0.6 MPa and temperatures between 1550 and 1650°C.
- The change in dimensions of the compressively crept specimens indicated that their size (both diameter and length) had actually increased as a consequence of the creep test conditions employed. The relatively large amount of expansion of the specimen diameters could not have been a sole consequence of "compressive creep barreling" because some specimens did not contract at all, and those that did, did not contract enough to cause a Poisson effect. All six brands showed this expansion effect. The increases in diameter and length of the creep specimens were between 0.35-1.0%. Only a fraction of this expansion was detected during the compressive creep testing. This indicates that most of the permanent expansion exhibited by these silica refractory creep specimens occurred during their heating from ambient to the creep testing temperature or during the cooling from it to ambient.
- The secondary phase constituents remained in all brands when they were tested at 1550°C (cumulative time at temperature approximately 250 hours). A fraction of these phases visibly

evolved from the specimens at 1600°C (slight glass bubbling on the specimen and fixturing). This phenomenon was quite severe at 1650°C. The density changes in the crept specimens (a net effect of the volume expansion and loss in secondary phase mass) ranged from a decrease of 1.6 to 3.9% with a subtle trend of greater density decreases at higher test temperatures. The density decreases among the six brands were statistically equivalent within the data scatter.

- The cause of the volume expansion was not identified; however, because of the absence of quartz it can be concluded that the expansion was not due to quartz (a relatively high density) converting to tridymite or cristobalite (lower density phases). The authors speculate that the volume expansion is due to the high temperature process of the conversion of tridymite to cristobalite and the consequential growth of the residual pores and the original cristobalite aggregates.
- Unstressed or "aged" silica refractory specimens from all six materials also exhibited loss of mass, dimensional increases, and density decreases between 1550-1650°C.
    - The mass losses of the six brands at 1550 and 1600°C were equivalent; however, some silica brands lost more mass than others at 1650°C: Harbison-Walker's developmental brand lost approximately 0.1% of its mass; SI96AU lost ≈ 0.2%; Vega H lost ≈ 0.3%; Gen-Sil lost ≈ 0.5%; Vega lost ≈ 1.0%; and Stella GGS lost ≈ 1.5%. The majority of the mass loss for all six brands occurred in less than 25 hours.
    - The dimensional increases of the silica specimens were a function of temperature. Additionally, some brands expanded more than others. The ranges of expansion were ≈ 1-2.5% at 1550°C, ≈ 2.25-3.75% at 1600°C, and ≈ 3.5-6% at 1650°C. Harbison-Walker's developmental brand expanded the least amount at all three temperatures followed by Gen-Sil. The ascending order of expansion for the other four brands varied with temperature. Stella GGS expanded the most at 1550°C (≈ 2.5%), SI96AU expanded the most at 1600°C (≈ 3.75%), and Vega expanded the most at 1650°C (≈ 6%). Dimensional increases in these aging specimens were greater than axial expansion of the crept silica specimens at the same temperatures indicating that the axially applied compressive load during creep testing resulted in some specimen contraction.

- The density decreases of the silica specimens were a function of temperature. Additionally, some brands became less dense than others. The changes in density are a consequence of the above described changes in mass and volume. The ranges of density decreases were ≈ 1-2.75% at 1550°C, ≈ 2.25-4.0% at 1600°C, and ≈ 3.5-7.0% at 1650°C. The density of Harbison-Walker's developmental brand changed the least of the six brands at all three temperatures. The ascending order of density for the other five brands varied with temperature. The density of Stella GGS decreased the most at 1550°C (≈ 2.75%), that for SI96AU decreased the most at 1600°C (≈ 4%), and that for Vega decreased the most at 1650°C (≈ 7%).

- The corrosion resistances of the six silicas were statistically equivalent when they were exposed to sodium carbonate at 1400°C (2550°F) for 24 hours. The amount of recession increased linearly with temperature between 1250-1450°C for the Gen-Sil silica.

6. REFERENCES

[1] Crown Refractories for Glass Manufacturing With Oxy-Fuel Combustion, Teltech Research Services, Minneapolis, MN, 1996.

[2] M. Gridley, "Philosophy, Design, and Performance of Oxy-Fuel Furnaces," *Ceramic Engineering and Science Proceedings*, **18** 1-14 (1997).

[3] R. W. Schroeder, "Development of Oxy-Fuel Technology in the Glass Industry," *the GlassResearcher*, NYSCC@Alfred University, **8** [1] 1-4 (1998).

[4] A. A. Wereszczak, "Which Superstructure Refractories Do Glassmakers Desire Creep Data For?" *Glass Industry*, pp. 17-18, 24, November (1998).

[5] "Standard Classification of Silica Refractory Brick," ASTM C416, Vol. 15.01, American Society for Testing and Materials, West Conshohocken, PA, 1998.

[6] "Standard Test Method of Measuring the Thermal Expansion and Creep of Refractories Under Load," ASTM C832, Vol. 15.01, American Society for Testing and Materials, West Conshohocken, PA, 1998.

[7] K. C. Liu, C. O. Stevens, C. R. Brinkman, and N.E. Holshauser, "A Technique to Achieve Uniform Stress Distribution in Compressive Creep Testing of Advanced Ceramics at High temperatures," *Journal of Engineering for Gas Turbines and Power*, **119** 500-505 (1997).

[8] K. C. Liu and J. L. Ding, "Mechanical Extensometer for High Temperature Tensile Testing of Ceramics," *Journal of Testing and Evaluation*, **21** 406-413 (1993).

[9] S. Shin and O. Buyukozturk, Material Property Development for Refractories, US DOE Report ORNL/Sub/79-07862/02 (1990).

[10] "Standard Test Method for Load Testing Refractory Brick at High Temperatures," ASTM C16, Vol. 15.01, American Society for Testing and Materials, West Conshohocken, PA, 1998.

[11] F. H. Norton, The Creep of Steel at High Temperature, McGraw Hill, New York, 1929.

[12] A. A. Wereszczak, T. P. Kirkland, and W. F. Curtis, "Creep of CaO/SiO_2-Containing MgO Refractories," In press, *Journal of Materials Science*, (1999).

[13] "Standard Practice for Vapor Attack on Refractories for Furnace Superstructures," ASTM C987, Vol. 15.01, American Society for Testing and Materials, West Conshohocken, PA, 1998.

[14] "Standard Test Method for Bulk Density and Volume of Solid Refractories by Wax Immersion," ASTM C914, Vol. 15.01, American Society for Testing and Materials, West Conshohocken, PA, 1998.

[15] M. Karakus and R. E. Moore, "CLM - A New Technique for Refractories," *Ceramic Bulletin*, 77 55-61 (1998).

Acknowledgments

The authors are indebted to

- the following individuals for supplying the conventional silica refractories: J. Conrad of A. P. Green; P. Antimarino of Harbison-Walker; R. Antram of NARCO; and D. J. Thomas of VGT-DYKO;
- the guidance provided by the Glass Industry Advisory Committee, which is comprised of the following individuals: P. Antimarino of Harbison-Walker; W. Curtis of PPG; L. Kotascka of Corning; M. Nelson of Corhart; A. Poolos of Owens-Brockway; J. Shell of Techneglas; and S. Winder of UKSS/Monofrax;
- the following individuals for reviewing the report and for their helpful comments: P. Antimarino of Harbison-Walker; W. Curtis of PPG; L. Kotacska and D. Liebner of Corning Glass; D. McIntyre of NARCO; J. G. Hemrick of the University of Missouri at Rolla; S. Winder of UKSS; and K. Breder, A. E. Pasto, and R. W. Swindeman of ORNL;
- ORNL/HTML machinists L. O'Rourke, T. Jenkins, and R. Parten for the specimen preparation; and
- DOE/OIT/AIM Program Manager C. Sorrell for his support of this project.

INTERNAL DISTRIBUTION

P. Angelini (7)
J. Ball
C. Beasley
P. Becher
T. Besmann
R. Bradley
K. Breder (4)
D. Craig
W. Hayden
T. Kirkland
K. Liu (4)
A. Pasto
B. Pint (4)
M. Rawlins
A. Schaffhauser
R. Swindeman
A. Wereszczak (30)
J. Young
Central Research Library
Laboratory Records, ORNL-RC (3)

EXTERNAL DISTRIBUTION

P. Antimarino
Harbison-Walker Refractories
600 Grant St.
Pittsburgh, PA 15219

T. Berg
CertainTeed
PO Box 1100
Blue Bell, PA 19446

R. Butters
Department of Energy, EE-24
1000 Independence Avenue, SW
Washington, DC 20585

M. Carroll
Knauf Fiber Glass GmbH
240 Elizabeth St.
Shelbyville, IN 46176

J. Ceriani
Kimball Glass Inc.
537 Crystal Avenue
Vineland, NJ 08360

M. Choudhary
Owens Corning
2790 Columbus Road
Granville, OH 43023

C. Cocagne
Guardian Industries Corp.
2300 Harmon Rd.
Auburn Hills, MI 48326

K. Congleton
American Video Glass Company
777 Technology Drive.
Mt. Pleasant, PA 15666

J. Conrad
AP Green Industries
1 Green Blvd.
Mexico, MO 65265

W. Curtis
PPG Industries, Inc.
Glass Technology Center
PO Box 11472
Harmerville, PA 15238

T. Dankert
Owens-Brockway
One Seagate Center, 30-LDP
Toledo, OH 43666

P. DeHoff
The PQ Corporation
Corporate Headquarters
PO Box 840
Valley Forge, PA 19482

K. Enos
Philips Lighting Co.
320 Vaksdahl Ave.
Danville, KY 40422

E. Flygt
Glass Research Institute
Box 3093
SE-350 33 Vaxjoe
SWEDEN

M. Greenman
Glass Manufacturing Industry Council
4633 Dapple Court
Ellicott City, MD 21043

M. Gridley
Ball-Foster Glass Container Co.
PO Box 4200
Muncie, IN 47307

M. Hanavan
Coors Glass - RMBC
10619 W. 50th Ave.
Wheatridge, CO 80033

V. Henry
Ford Motor Company
15000 Commerce Dr. North
Dearborn, MI 48120

T. Hoffman
Osram Sylvania Inc.
1000 Tyrone Park
Versailles, KY 40383

W. Horan
Techneglas, Inc.
60 Old Boston Road
Pittston, PA 18640

J. Houp
National Refractories & Minerals
41738 Esterly Drive
PO Box 47
Columbiana, OH 44408-0047

S. Hutchins
Glenshaw Glass Company
1101 William Flynn Highway
Glenshaw, PA 15116

P. Hutchinson
DSF Refractories & Minerals Ltd.
Friden, Newhaven, NR Buxton
Derbyshire SK17 0DX
England, UK

K. Hyrcik
General Electric Lighting
Nela Par Noble Rd.
East Cleveland, OH 44112

R. Jain
Department of Energy, EE-24
1000 Independence Avenue, SW
Washington, DC 20585

C. Jian
Owens Corning
2790 Columbus Road
Granville, OH 43023

T. Johnson
Department of Energy, EE-21
1000 Independence Avenue, SW
Washington, DC 20585

M. Karakus (4)
University of Missouri @ Rolla
Ceramic Engineering Dept.
222 McNutt Hall
Rolla, MO 65409

D. Kauser
Pittsburgh Corning
800 Presque Isle Dr.
Pittsburgh, PA 15239-2799

L. Kotacska
Corning Incorporated
HP-ME-02-038
Corning, NY 14831

J. Kynik
St. George Crystal
Brown Ave., PO Box 709
Jeannette, PA 15644

J. LeBlanc
BOC Gases
1720 Indian Wood Circle
Maumee, OH 43537

D. Liebner
Corning Incorporated
HP-ME-02-038
Corning, NY 14831

A. Link
Lancaster Glass Corporation
240 West Main St.
PO Box 70
Lancaster, OH 43130-0070

K. Lombardi
Holophane Corporation
PO Box 3004
214 Oakwood Avenue
Newark, OH 43058-3004

D. Lubelski
Pilkington LOF
1701 East Broadway
Toledo, OH 43605

W. McCullah, Jr.
AFG Industries
PO Box 929
Kingsport, TN 37662

J. McGaughey
Libbey Inc.
PO Box 919
Toledo, OH 43616

D. McIntyre
North American Refractories
3127 Research Dr.
State College, PA 16801

T. Merdian
Premier Refractories
27 Noblestown Road
Carnegie, PA 15106

D. Moore
Gallo Glass
Box 1230
Modesto, CA 95353

R. Moore (4)
University of Missouri @ Rolla
Ceramic Engineering Dept.
224 McNutt Hall
Rolla, MO 65409

M. Nelson
Corhart Refractories
1600 West Lee St.
Louisville, KY 40210

M. Nowson
Anchor Glass
4343 Anchor Plaza Pike
Tampa, FL 33634

G. Pecoraro
PPG Industries Inc.
Glass Technology Center
PO Box 11472
Pittsburgh, PA 15238-0472

J. Petreanu
Owens Corning
Science & Technology Center
2790 Columbus Rd.
Granville, OH 43023

M. Piper
Cardinal FG
2200 Parkway Drive
Menomonie, WI 54751

A. Poolos
Owens-Brockway Inc.
1 Seagate 30L/GC
Toledo, OH 43666

F. Quan
Corning, Inc.
Sullivan Park FR-2
Corning, NY 14831

P. Ross
GICI
PO Box 6730
Lagons Miguel, CA 92607-6730

W. Schaub
BNZ Materials
924 Cadwell Ave
Elmhurst, IL 60126

D. Shamp
Schuller International, Inc.
PO Box 517
Toledo, OH 43697-0517

J. Shell
Techneglas
727 E. Jenkins Ave.
Columbus, OH 43207

M. Smith
Department of Energy, EE-23
1000 Independence Avenue, SW
Washington, DC 20585

C. Sorrell
Department of Energy, EE-23
1000 Independence Avenue, SW
Washington, DC 20585

M. Stett
National Refractories & Minerals Corp.
1852 Rutan Dr.
Livermore, CA 94550

L. Stover
Minteq International, Inc.
PO Box 446
Dover, OH 44622

D. Thomas
VGT-DYKO Industrial Ceramics Inc.
7002 Graymoor Rd.
Louisville, KY 40222

D. VerDow
Thomson Consumer Electronics
24200 US 23 South
Circleville, OH 43130

S. Winder
UK Software Services Inc.
30 Hemlock Drive
Grand Island, NY 14072

H. Winkelbauer
Harbison-Walker Refractories Co.
1001 Pittsburgh-McKeesport Blvd.
West Mifflin, PA 15512-2289